

A DERIVATIVE-ORTHOGONAL WAVELET MULTISCALE METHOD FOR 1D ELLIPTIC EQUATIONS WITH ROUGH DIFFUSION COEFFICIENTS

QIWEI FENG AND BIN HAN

ABSTRACT. In this paper, we investigate 1D elliptic equations $-\nabla \cdot (a\nabla u) = f$ with rough diffusion coefficients a that satisfy $0 < a_{\min} \leq a \leq a_{\max} < \infty$ and $f \in L_2(\Omega)$. To achieve an accurate and robust numerical solution on a coarse mesh of size H , we introduce a derivative-orthogonal wavelet-based framework. This approach incorporates both regular and specialized basis functions constructed through a novel technique, defining a basis function space that enables effective approximation. We develop a derivative-orthogonal wavelet multiscale method tailored for this framework, proving that the condition number κ of the stiffness matrix satisfies $\kappa \leq a_{\max}/a_{\min}$, independent of H . For the error analysis, we establish that the energy and L_2 -norm errors of our method converge at first-order and second-order rates, respectively, for any coarse mesh H . Specifically, the energy and L_2 -norm errors are bounded by $2a_{\min}^{-1/2} \|f\|_{L_2(\Omega)} H$ and $4a_{\min}^{-1} \|f\|_{L_2(\Omega)} H^2$. Moreover, the numerical approximated solution also possesses the interpolation property at all grid points. We present a range of challenging test cases with continuous, discontinuous, high-frequency, and high-contrast coefficients a to evaluate errors in u, u' and au' in both l_2 and l_∞ norms. We also provide a numerical example that both coefficient a and source term f contain discontinuous, high-frequency and high-contrast oscillations. Additionally, we compare our method with the standard second-order finite element method to assess error behaviors and condition numbers when the mesh is not fine enough to resolve coefficient oscillations. Numerical results confirm the bounded condition numbers and convergence rates, affirming the effectiveness of our approach. Thus, our method is capable of handling both the rough diffusion coefficient a and the rough source term f , provided that $\|f\|_{L_2(\Omega)}$ is not huge.

1. INTRODUCTION AND PROBLEM FORMULATION

The elliptic problems with rough, discontinuous, high-contrast, and high-frequency diffusion coefficients arise in many real-world applications ([1, 3–5, 7, 13, 20, 27, 38, 40]), such as the demanding SPE10 (Society of Petroleum Engineers 10) benchmark problem. The discontinuities, high-contrast jumps, and high frequencies result from the permeability variations in the different geological layers of the SPE10 problem [41]. Usually, the solution of the elliptic equation with the rough diffusion coefficient contains severe singularities (see e.g. [6, 8, 11, 22–26, 32, 33, 35, 36]). Since diffusion coefficients typically exhibit high-frequency oscillations and encompass multiple spatial scales, employing the standard finite element and finite volume methods with linear basis functions necessitates the fine grid mesh to capture small-scale features of coefficients. This requirement of using very fine meshes leads to the high computational cost and large stiffness matrices. To obtain a reliable and precise solution with the detailed oscillation on the coarse mesh size, various multiscale methods are proposed (see e.g. [2, 9, 10, 12, 16–19, 21, 28–30, 34, 37, 39, 42]).

In this paper, we discuss the following 1D elliptic equation with the rough diffusion coefficient in the domain $\Omega := (0, 1)$:

$$\begin{cases} -\nabla \cdot (a\nabla u) = f & \text{in } \Omega, \\ u = 0 & \text{on } \partial\Omega. \end{cases} \quad (1.1)$$

2010 *Mathematics Subject Classification.* 65N30, 35J15, 76S05.

Key words and phrases. Elliptic equations, rough coefficients, derivative-orthogonal wavelets, multiscale methods, bounded condition numbers, error estimates.

Research supported in part by the Mathematics Research Center, Department of Mathematics, University of Pittsburgh, Pittsburgh, PA, USA and Natural Sciences and Engineering Research Council (NSERC) of Canada under grants RGPIN-2024-04991.

We investigate the model problem (1.1) only under the following two assumptions:

- (A1) There exist positive constants $a_{\min} = \inf_{x \in \Omega} a(x)$ and $a_{\max} = \sup_{x \in \Omega} a(x)$ such that $0 < a_{\min} \leq a \leq a_{\max} < \infty$ in Ω .
- (A2) The source term $f \in L_2(\Omega)$.

The weak formulation of the equation (1.1) is to find $u \in H_0^1(\Omega)$ such that

$$\int_{\Omega} a \nabla u \cdot \nabla v = \int_{\Omega} f v, \quad \text{for all } v \in H_0^1(\Omega). \quad (1.2)$$

The organization of this paper is as follows.

In Section 2.1, we utilize derivative-orthogonal wavelets to construct regular basis functions. In Section 2.2, we propose a novel algorithm to develop special basis functions. In Section 2.3, we define our basis function spaces by regular and special basis functions, and then derive our derivative-orthogonal wavelet multiscale method. In Theorem 2.2 of Section 2.4, we prove that the condition number of the stiffness matrix of our derivative-orthogonal wavelet multiscale method is bounded by a_{\max}/a_{\min} for any coarse mesh size H . In Section 2.5, we derive Theorem 2.5 and Theorem 2.6 to theoretically prove that the energy and L_2 -norm errors of our method converge at first-order and second-order rates, respectively, for any coarse mesh H . Specifically, the energy and L_2 -norm errors are bounded by $C_1 H$ and $C_2 H^2$ with $C_1 = 2\|f\|_{L_2(\Omega)}/\sqrt{a_{\min}}$ and $C_2 = 4\|f\|_{L_2(\Omega)}/a_{\min}$. We shall also prove in Theorem 2.8 that the numerical approximated solution also possesses the interpolation property at all grid points.

In Section 3, we provide numerical experiments to verify convergence rates measured in l_2 and l_{∞} norms. We test numerical examples in the following 6 cases:

- Example 1: u is available and a is continuous with high-frequency oscillations in Ω .
- Example 2: u is available and a is discontinuous with high-contrast jumps in Ω .
- Example 3: u is available, a is continuous with high-frequency oscillations, $\lim_{x \rightarrow 0^+} a(x) = \infty$.
- Example 4: u is unavailable and a is continuous with high-frequency oscillations in Ω .
- Example 5: u is unavailable and a is discontinuous with high-contrast jumps in Ω .
- Example 6: u is unavailable, a and f are both discontinuous with high-contrast jumps and high-frequency oscillations in Ω .

In Examples 1 to 3, we compare our proposed derivative-orthogonal wavelet multiscale method with the standard second-order finite element method.

In Section 4, we summarize the main contributions of our paper.

2. THE DERIVATIVE-ORTHOGONAL WAVELET MULTISCALE METHOD

We now describe our proposed derivative-orthogonal wavelet multiscale method to solve (1.1).

2.1. Regular basis functions. In this subsection, we construct regular basis functions by using derivative-orthogonal wavelets [15] as follows:

$$\phi(x) = \begin{cases} x + 1, & x \in [-1, 0), \\ 1 - x, & x \in [0, 1), \\ 0, & \text{else,} \end{cases} \quad \psi(x) = \begin{cases} 2x, & x \in [0, \frac{1}{2}), \\ 2 - 2x, & x \in [\frac{1}{2}, 1), \\ 0, & \text{else.} \end{cases} \quad (2.1)$$

Then

$$\phi(2x - 1) = \begin{cases} 2x, & x \in [0, \frac{1}{2}), \\ 2 - 2x, & x \in [\frac{1}{2}, 1), \\ 0, & \text{else,} \end{cases} \quad (\phi(2x - 1))' = \begin{cases} 2, & x \in [0, \frac{1}{2}), \\ -2, & x \in [\frac{1}{2}, 1), \\ 0, & \text{else,} \end{cases} \quad (2.2)$$

and

$$\psi(2^j x - k) = \begin{cases} 2^{j+1}x - 2k, & x \in [\frac{k}{2^j}, \frac{1/2+k}{2^j}), \\ 2 - 2^{j+1}x + 2k, & x \in [\frac{1/2+k}{2^j}, \frac{1+k}{2^j}), \\ 0, & \text{else,} \end{cases} \quad (\psi(2^j x - k))' = \begin{cases} 2^{j+1}, & x \in [\frac{k}{2^j}, \frac{1/2+k}{2^j}), \\ -2^{j+1}, & x \in [\frac{1/2+k}{2^j}, \frac{1+k}{2^j}), \\ 0, & \text{else,} \end{cases} \quad (2.3)$$

where $k = 0, \dots, 2^j - 1$ and $j = 1, \dots, n - 1$ with $n \in \mathbb{N}$ and $n \geq 2$. Now, we define the derivative-orthogonal wavelet space $V_H := \text{span}(\mathcal{B}_H)$ with the uniform coarse mesh size H as follows:

$$\mathcal{B}_H := \{\phi(2x - 1)\} \cup \{\psi(2^j x - k) : k = 0, \dots, 2^j - 1, j = 1, \dots, n - 1\}, \quad (2.4)$$

where $H = 1/2^n$ for an integer $n \geq 2$. See Figs. 1 to 4 for illustrations of $\{\phi(2x - 1)\}$, $\{\psi(2^j x - k) : k = 0, \dots, 2^j - 1\}$, $\{(\phi(2x - 1))'\}$, $\{(\psi(2^j x - k))' : k = 0, \dots, 2^j - 1\}$ with $j = 1, 2$. Clearly,

$$V_H := \text{span}(\mathcal{B}_H) \subset H_0^1(\Omega). \quad (2.5)$$

Let $\text{supp}(f)$ denote the support of the function f . By (2.3), the elements in the basis \mathcal{B}_H satisfy

$$\begin{aligned} \text{supp}((\psi(2^j x - k_0))') \cap \text{supp}((\phi(2x - 1))') &= \text{supp}((\psi(2^j x - k_0))') \quad \text{or} \quad \emptyset, \\ \text{supp}((\psi(2^j x - k_1))') \cap \text{supp}((\psi(2^j x - k_2))') &= \emptyset, \quad \text{if } k_1 \neq k_2, \end{aligned} \quad (2.6)$$

for any $k_0, k_1, k_2 = 0, \dots, 2^j - 1$ and $j = 1, \dots, n - 1$. Furthermore, for any $1 \leq j_1 \leq j_2$ with $j_1, j_2 \in \mathbb{N}$,

$$\text{supp}((\psi(2^{j_1} x - k_1))') \cap \text{supp}((\psi(2^{j_2} x - k_2))') = \text{supp}((\psi(2^{j_2} x - k_2))') \quad \text{or} \quad \emptyset, \quad (2.7)$$

where $k_1 = 0, \dots, 2^{j_1} - 1$ and $k_2 = 0, \dots, 2^{j_2} - 1$.

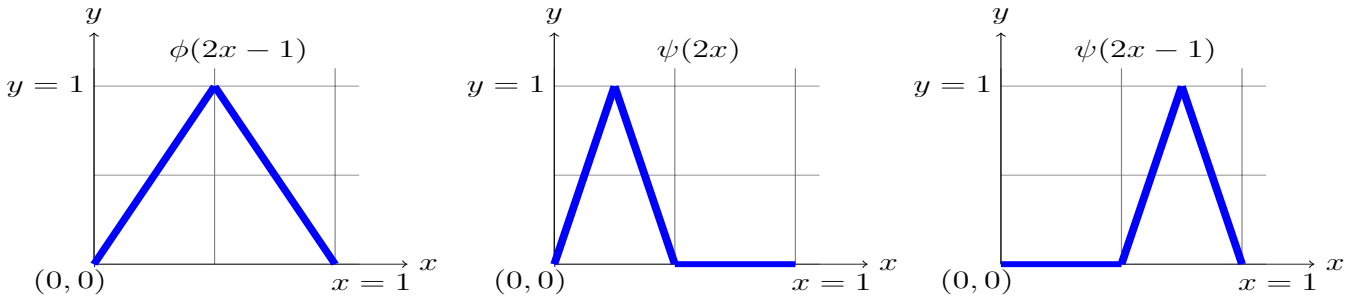


FIGURE 1. Left panel: $\phi(2x - 1)$. Middle and right panels: $\{\psi(2^j x - k) : k = 0, \dots, 2^j - 1\}$ with $j = 1$.

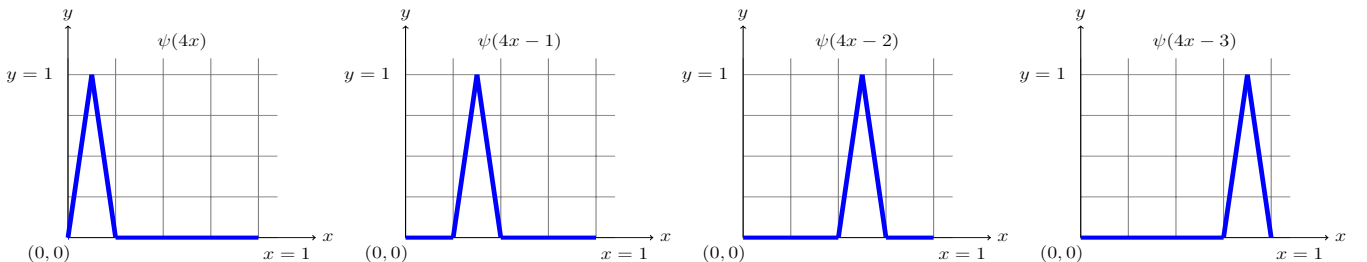


FIGURE 2. $\{\psi(2^j x - k) : k = 0, \dots, 2^j - 1\}$ with $j = 2$.

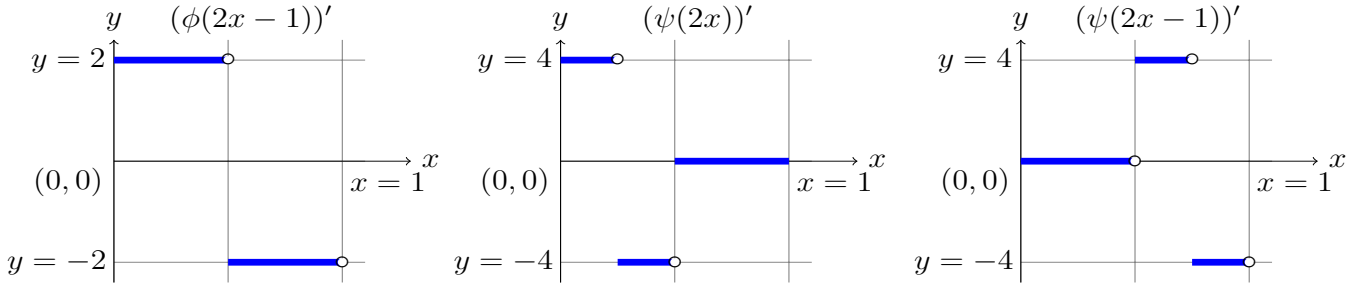


FIGURE 3. Left panel: $(\phi(2x-1))'$. Middle and right panels: $\{(\psi(2^j x - k))' : k = 0, \dots, 2^j - 1\}$ with $j = 1$.

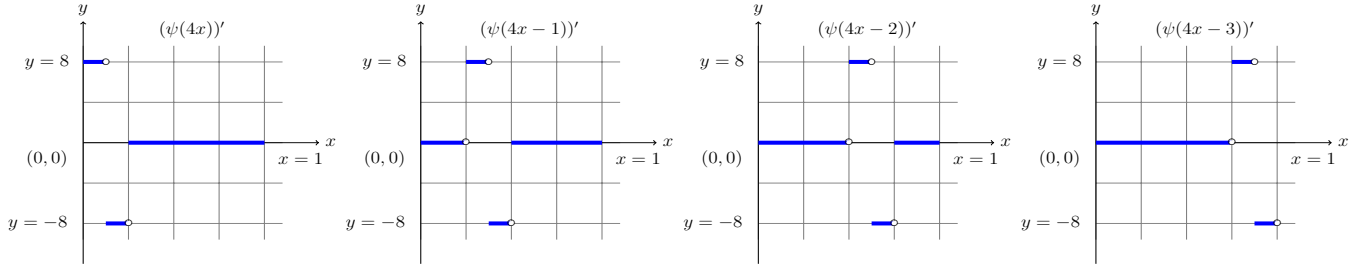


FIGURE 4. $\{(\psi(2^j x - k))' : k = 0, \dots, 2^j - 1\}$ with $j = 2$.

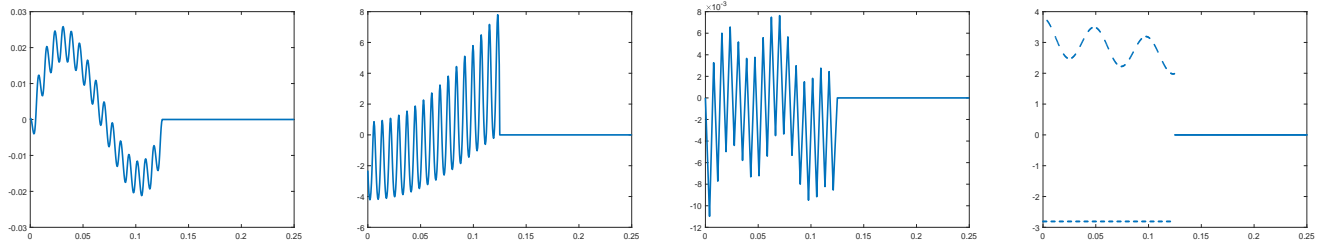


FIGURE 5. S_0 (first panel) and $(S_0)'$ (second panel) in (2.9) with $n = 3$ in $[0, \frac{1}{4}]$ with a continuous coefficient function a . S_0 (third panel) and $(S_0)'$ (fourth panel) in (2.9) with $n = 3$ in $[0, \frac{1}{4}]$ with a discontinuous coefficient function a . Note that $\overline{\text{supp}(S_0)} = \overline{\text{supp}((S_0)')} = [0, \frac{1}{8}]$ in the above two S_0 .

2.2. Special basis functions. To capture the high-contrast jump and the high-frequency oscillation of the coefficient on the coarse mesh size H , in this subsection, besides regular basis functions, we also construct special basis functions (see Fig. 5 for an illustration) by solving the following equations

$$\begin{cases} (S_i)'' = \left(\frac{1}{a}\right)', & x \in \left(\frac{i}{2^n}, \frac{i+1}{2^n}\right), \\ S_i = 0, & x \in \left[0, \frac{i}{2^n}\right] \cup \left[\frac{i+1}{2^n}, 1\right], \end{cases} \quad (2.8)$$

where $i = 0, \dots, 2^n - 1$ for an integer $n \geq 2$. For the sake of brevity, we construct special basis functions by using the following equivalent formula of (2.8):

$$S_i = \begin{cases} \int_{\frac{i}{2^n}}^x \left(\frac{1}{a(t)} - w_i\right) dt, & x \in \left(\frac{i}{2^n}, \frac{i+1}{2^n}\right), \\ 0, & x \in \left[0, \frac{i}{2^n}\right] \cup \left[\frac{i+1}{2^n}, 1\right], \end{cases} \quad (2.9)$$

where $i = 0, \dots, 2^n - 1$ for an integer $n \geq 2$ and

$$w_i = \frac{\int_{\frac{i}{2^n}}^{\frac{i+1}{2^n}} \frac{1}{a(t)} dt}{\frac{i+1}{2^n} - \frac{i}{2^n}} = 2^n \int_{\frac{i}{2^n}}^{\frac{i+1}{2^n}} \frac{1}{a(t)} dt. \quad (2.10)$$

Then (2.9) and (2.10) yield

$$S_i \left(\frac{i}{2^n} \right) = 0, \quad (2.11)$$

$$S_i \left(\frac{i+1}{2^n} \right) = \int_{\frac{i}{2^n}}^{\frac{i+1}{2^n}} \left(\frac{1}{a(t)} - w_i \right) dt = \int_{\frac{i}{2^n}}^{\frac{i+1}{2^n}} \frac{1}{a(t)} dt - \frac{w_i}{2^n} = 0, \quad (2.12)$$

and

$$(S_i)' = \begin{cases} \frac{1}{a} - w_i, & x \in \left[\frac{i}{2^n}, \frac{i+1}{2^n} \right), \\ 0, & \text{else,} \end{cases} \quad (2.13)$$

where $i = 0, \dots, 2^n - 1$ for an integer $n \geq 2$. So

$$\text{supp}((S_i)') \cap \text{supp}((S_j)') = \emptyset, \quad \text{if } i \neq j. \quad (2.14)$$

According to $a > 0$, if a is not a constant function on $\left(\frac{i}{2^n}, \frac{i+1}{2^n} \right)$, we observe

$$\|(S_i)'\|_{L_2(\Omega)}^2 = \int_{\frac{i}{2^n}}^{\frac{i+1}{2^n}} \left(\frac{1}{a} - w_i \right)^2 dx > 0.$$

Note that we throw away S_i if a is a constant on $\left(\frac{i}{2^n}, \frac{i+1}{2^n} \right)$ because $S_i = 0$. Clearly,

$$\|(\phi(2x-1))'\|_{L_2(\Omega)}^2 = 4 \quad \text{and} \quad \|(\psi(2^j x - k))'\|_{L_2(\Omega)}^2 = \frac{2^{2j+3}}{2^{j+1}} = 2^{j+2}.$$

2.3. The proposed derivative-orthogonal wavelet multiscale method. Now, we formulate the derivative-orthogonal wavelet multiscale method space with defined regular (Section 2.1) and special (Section 2.2) basis functions in the uniform coarse mesh size H as follows:

$$\begin{aligned} \tilde{\mathcal{B}}_H = & \left\{ \frac{\phi(2x-1)}{\|(\phi(2x-1))'\|_{L_2(\Omega)}} \right\} \cup \left\{ \frac{\psi(2^j x - k)}{\|(\psi(2^j x - k))'\|_{L_2(\Omega)}} : k = 0, \dots, 2^j - 1, j = 1, \dots, n-1 \right\} \\ & \cup \left\{ \frac{S_i}{\|(S_i)'\|_{L_2(\Omega)}} : i = 0, \dots, 2^n - 1 \right\}, \end{aligned} \quad (2.15)$$

where $H = 1/2^n$ for an integer $n \geq 2$. Note that $\|g'\|_{L_2(\Omega)} = 1$ for every $g \in \tilde{\mathcal{B}}_H$ and

$$\tilde{V}_H := \text{span}(\tilde{\mathcal{B}}_H) \subset H_0^1(\Omega). \quad (2.16)$$

By (2.2) and (2.13),

$$\begin{aligned} [0, \frac{1}{2}] \cap \text{supp}((S_i)') &= \text{supp}((S_i)') \quad \text{or} \quad \emptyset, \\ [\frac{1}{2}, 1] \cap \text{supp}((S_i)') &= \text{supp}((S_i)') \quad \text{or} \quad \emptyset, \end{aligned} \quad (2.17)$$

where $i = 0, \dots, 2^n - 1$ and $n \geq 2$. (2.3) and (2.13) imply

$$\begin{aligned} \left[\frac{k}{2^j}, \frac{k+1/2}{2^j} \right] \cap \text{supp}((S_i)') &= \text{supp}((S_i)') \quad \text{or} \quad \emptyset, \\ \left[\frac{k+1/2}{2^j}, \frac{k+1}{2^j} \right] \cap \text{supp}((S_i)') &= \text{supp}((S_i)') \quad \text{or} \quad \emptyset, \end{aligned} \quad (2.18)$$

where $k = 0, \dots, 2^j - 1$, $j = 1, \dots, n-1$, $i = 0, \dots, 2^n - 1$ and $n \geq 2$. For the sake of brevity, we rewrite $\tilde{\mathcal{B}}_H$ in (2.15) as

$$\tilde{V}_H = \text{span}(\tilde{\mathcal{B}}_N) \quad \text{and} \quad \tilde{\mathcal{B}}_N = \{\varphi_1, \varphi_2, \dots, \varphi_M\}, \quad (2.19)$$

where

$$M = 1 + \left(\sum_{j=1}^{n-1} \sum_{k=0}^{2^j-1} 1 \right) + 2^n = 1 + \left(\sum_{j=1}^{n-1} 2^j \right) + 2^n = 1 + \frac{2-2^n}{1-2} + 2^n = 2^{n+1} - 1. \quad (2.20)$$

Now, the numerical solution of our proposed derivative-orthogonal wavelet multiscale method is computed by the following procedure: Find $\tilde{u}_H \in \tilde{V}_H := \text{span}(\tilde{\mathcal{B}}_H)$ such that

$$\int_{\Omega} a \nabla \tilde{u}_H \cdot \nabla \tilde{v}_H = \int_{\Omega} f \tilde{v}_H, \quad \text{for all } \tilde{v}_H \in \tilde{\mathcal{B}}_H, \quad (2.21)$$

where $\tilde{\mathcal{B}}_H$ is defined in (2.15) or equivalently (2.19) and is the basis of \tilde{V}_H with the derivative-orthogonality property ([15]). See [14, 15] and many references therein for wavelet-based applications for numerical PDEs. Note that $\mathcal{B}_H \subset \tilde{\mathcal{B}}_H$, while $\mathcal{B}_{H/2}$ and $\tilde{\mathcal{B}}_H$ have the same cardinality $2^{n+1} - 1$.

2.4. Bounded condition numbers. In this subsection, we first state the following Lemma 2.1 which is used to prove that the condition number of our proposed derivative-orthogonal wavelet multiscale method is bounded by a_{\max}/a_{\min} .

Lemma 2.1. *For any φ_i and $\varphi_j \in \tilde{\mathcal{B}}_H$,*

$$\int_{\Omega} (\varphi_i)'(\varphi_j)' dx = \delta_{ij}, \quad (2.22)$$

where $\tilde{\mathcal{B}}_H$ is defined in (2.15) and (2.19). Hence, $\tilde{\mathcal{B}}_H$ forms a derivative-orthogonal basis of \tilde{V}_H .

Proof. By (2.2)–(2.7), we deduce

$$\int_{\Omega} (\varphi_i)'(\varphi_j)' = 0, \quad \text{if } \varphi_i \neq \varphi_j, \quad \text{for any } \varphi_i, \varphi_j \in \mathcal{B}_H,$$

where \mathcal{B}_H is defined in (2.4). Using (2.2), we obtain that for any S_i in (2.9)

$$\int_{\Omega} (\phi(2x-1))'(S_i)' dx = 2 \int_0^{1/2} (S_i)' dx - 2 \int_{1/2}^1 (S_i)' dx.$$

Note that (2.13) implies $\text{supp}((S_i)') \subset [0, 1/2]$ or $[1/2, 1]$. Then

$$\begin{aligned} \int_0^{1/2} (S_i)' dx &= \int_{\frac{i}{2^n}}^{\frac{i+1}{2^n}} (S_i)' dx \quad \text{or} \quad 0, \\ \int_{1/2}^1 (S_i)' dx &= \int_{\frac{i}{2^n}}^{\frac{i+1}{2^n}} (S_i)' dx \quad \text{or} \quad 0. \end{aligned}$$

Note that (2.11) and (2.12) result in

$$\int_{\frac{i}{2^n}}^{\frac{i+1}{2^n}} (S_i)' dx = S_i \left(\frac{i+1}{2^n} \right) - S_i \left(\frac{i}{2^n} \right) = 0. \quad (2.23)$$

So

$$\int_{\Omega} (\phi(2x-1))'(S_i)' dx = 0, \quad \text{for any } i = 0, \dots, 2^n - 1.$$

On the other hand, by (2.3),

$$\int_{\Omega} (\psi(2^j x - k))'(S_i)' dx = 2^{j+1} \int_{\frac{k}{2^j}}^{\frac{1/2+k}{2^j}} (S_i)' dx - 2^{j+1} \int_{\frac{1/2+k}{2^j}}^{\frac{1+k}{2^j}} (S_i)' dx.$$

Now (2.18) yields

$$\int_{\Omega} (\psi(2^j x - k))'(S_i)' dx = \begin{cases} 2^{j+1} \int_{\frac{k}{2^j}}^{\frac{1/2+k}{2^j}} (S_i)' dx = 2^{j+1} \int_{\frac{i}{2^n}}^{\frac{i+1}{2^n}} (S_i)' dx, & \text{supp}((S_i)') \subset [\frac{k}{2^j}, \frac{1/2+k}{2^j}], \\ -2^{j+1} \int_{\frac{1/2+k}{2^j}}^{\frac{1+k}{2^j}} (S_i)' dx = -2^{j+1} \int_{\frac{i}{2^n}}^{\frac{i+1}{2^n}} (S_i)' dx, & \text{supp}((S_i)') \subset [\frac{1/2+k}{2^j}, \frac{1+k}{2^j}], \\ 0, & \text{else.} \end{cases}$$

From (2.23), we observe

$$\int_{\Omega} (\psi(2^j x - k))' (S_i)' dx = 0.$$

Recall (2.14) that $\text{supp}((S_i)') \cap \text{supp}((S_j)') = \emptyset$ if $i \neq j$. Now, we can conclude that

$$\int_{\Omega} (\varphi_i)' (\varphi_j)' dx = 0, \quad \text{if } \varphi_i \neq \varphi_j \quad \text{for any } \varphi_i, \varphi_j \in \tilde{\mathcal{B}}_H.$$

By the definition of $\tilde{\mathcal{B}}_H$ in (2.15), it is straightforward to verify

$$\int_{\Omega} (\varphi_i)' (\varphi_i)' dx = 1, \quad \text{for any } \varphi_i \in \tilde{\mathcal{B}}_H.$$

Thus, (2.22) is proved. \square

Applying (2.22) in Lemma 2.1, the following theorem presents that the condition number κ of our proposed derivative-orthogonal wavelet multiscale method satisfies $\kappa \leq a_{\max}/a_{\min}$.

Theorem 2.2. *Define $a_{\max} := \sup_{x \in \Omega} a(x)$ and $a_{\min} := \inf_{x \in \Omega} a(x)$. Suppose that $0 < a_{\min} \leq a(x) \leq a_{\max} < \infty$ for all $x \in \Omega$. Let A be the corresponding stiffness matrix of (2.21) and κ be its condition number by using the basis $\tilde{\mathcal{B}}_H$ defined in (2.15) of \tilde{V}_H . Then A is an $M \times M$ symmetric positive definite matrix and*

$$\kappa \leq \frac{a_{\max}}{a_{\min}}, \quad (2.24)$$

where $M := 2^{n+1} - 1$ and n is an integer such that the uniform mesh size $H = 1/2^n$ and $n \geq 2$.

Proof. Note that $\tilde{\mathcal{B}}_H = \{\varphi_1, \dots, \varphi_M\}$ in (2.19). By (2.15), (2.16), and (2.21), we have

$$A_{ij} = \int_{\Omega} a(x) (\varphi_i)' (\varphi_j)' dx, \quad i, j = 1, \dots, M.$$

Let $c = (c_1, \dots, c_M)^T \in \mathbb{R}^M$ be a column vector with each $c_i \in \mathbb{R}$. Then

$$c^T A c = \int_{\Omega} a(x) \left(\sum_{i=1}^M c_i (\varphi_i)' \right) \left(\sum_{j=1}^M c_j (\varphi_j)' \right) dx = \int_{\Omega} a(x) \left(\sum_{i=1}^M c_i (\varphi_i)' \right)^2 dx.$$

By $0 < a_{\min} \leq a(x) \leq a_{\max} < \infty$ for all $x \in \Omega$ and $(\sum_{i=1}^M c_i (\varphi_i)')^2 \geq 0$, we conclude that

$$a_{\min} \int_{\Omega} \left(\sum_{i=1}^M c_i (\varphi_i)' \right)^2 dx \leq c^T A c \leq a_{\max} \int_{\Omega} \left(\sum_{i=1}^M c_i (\varphi_i)' \right)^2 dx.$$

As each $c_i \in \mathbb{R}$ and note that $\|(\varphi_i)'\|_{L^2(\Omega)}^2 = 1$ for any $\varphi_i \in \tilde{\mathcal{B}}_H$ in (2.15), we conclude from (2.22) in Lemma 2.1 that

$$\int_{\Omega} \left(\sum_{i=1}^M c_i (\varphi_i)' \right)^2 dx = \int_{\Omega} \sum_{i=1}^M \left(c_i (\varphi_i)' \right)^2 dx = \sum_{i=1}^M (c_i)^2.$$

Consequently, we proved

$$a_{\min} \sum_{i=1}^M (c_i)^2 \leq c^T A c \leq a_{\max} \sum_{i=1}^M (c_i)^2, \quad \forall c = (c_1, \dots, c_M)^T \in \mathbb{R}^M.$$

Now, we can see that the stiffness matrix A is a symmetric positive definite matrix, which implies the unique expression of $\tilde{u}_H \in \text{span}(\tilde{\mathcal{B}}_H)$ by solving (2.21). Now we conclude from the inequalities that the maximum and minimum eigenvalues of the matrix A satisfy that $\lambda_{\max} \leq a_{\max}$ and $\lambda_{\min} \geq a_{\min}$. Thus $\kappa = \lambda_{\max}/\lambda_{\min} \leq a_{\max}/a_{\min}$. \square

2.5. Error estimates. In this subsection, we theoretically prove that the energy and L_2 norms of the errors of our proposed method achieve first-order and second-order convergence rates in Theorem 2.5 and Theorem 2.6, respectively for any coarse mesh size H . To do so, we need the following auxiliary results in Lemma 2.3 and Lemma 2.4.

Lemma 2.3. *Let p be any piecewise constant function on Ω given by*

$$p(x) = p_i \in \mathbb{R}, \text{ for all } x \in [\frac{i}{2^n}, \frac{i+1}{2^n}) \text{ and } i = 0, \dots, 2^n - 1,$$

where n is a positive integer with $n \geq 2$. Then the function $p(x)$ can be uniquely expressed as

$$p(x) = c_0 + c_1(\phi(2x - 1))' + \sum_{j=1}^{n-1} \sum_{k=0}^{2^j-1} c_{j,k}(\psi(2^j x - k))', \quad (2.25)$$

where $(\phi(2x - 1))'$ and $(\psi(2^j x - k))'$ are defined in (2.2) and (2.3) respectively, and

$$c_0 = \frac{p_i}{2^n}, \quad c_1 = \frac{1}{4} \int_0^1 p(x)(\phi(2x - 1))' dx, \quad c_{j,k} = \frac{1}{2^{j+2}} \int_0^1 p(x)(\psi(2^j x - k))' dx.$$

Proof. The claim follows immediately from the facts that $\{(\psi(2^j x - k))' : j \in \mathbb{N}, 0 \leq k \leq 2^j - 1\} \cup \{(\phi(2x - 1))'\} \cup \{\chi_{[0,1]}\}$ form an orthogonal basis in $L_2(\Omega)$ and $\int_{\Omega} p(x)(\psi(2^j x - k))' dx = 0$ for all $j \geq n$ and $0 \leq k \leq 2^j - 1$. \square

In order to theoretically prove the convergence rate of the error in the energy norm of our proposed derivative-orthogonal wavelet multiscale method in Theorem 2.5, we define

$$\mathcal{B}'_H := \{\chi_{\Omega}\} \cup \{g' : g \in \mathcal{B}_H\} \quad \text{and} \quad \tilde{\mathcal{B}}'_H := \{\chi_{\Omega}\} \cup \{g' : g \in \tilde{\mathcal{B}}_H\}, \quad (2.26)$$

where \mathcal{B}_H and $\tilde{\mathcal{B}}_H$ are defined in (2.4) and (2.15), respectively, and $H = 1/2^n$ for an integer $n \geq 2$.

Lemma 2.4. *For any $f_1, f_2 \in \text{span}(\mathcal{B}'_H)$ and $f_3 \in \text{span}(\tilde{\mathcal{B}}'_H)$, we have*

$$f_1 f_2 \in \text{span}(\mathcal{B}'_H), \quad f_1 f_3 \in \text{span}(\tilde{\mathcal{B}}'_H), \quad \text{and} \quad \text{span}(\mathcal{B}'_H) \subset \text{span}(\tilde{\mathcal{B}}'_H). \quad (2.27)$$

Proof. (2.27) can be directly derived from (2.2)–(2.7), (2.15)–(2.18), and (2.26). \square

With the aid of Lemma 2.3, Lemma 2.4, and (2.26), we prove that the first-order convergence rate of the error in the energy norm of our proposed method can be achieved for any coarse mesh size H in the following Theorem 2.5.

Theorem 2.5. *Define $a_{\max} := \sup_{x \in \Omega} a(x)$ and $a_{\min} := \inf_{x \in \Omega} a(x)$. Let u be the exact solution of the model problem (1.1) under the assumptions that $0 < a_{\min} \leq a \leq a_{\max} < \infty$ and $f \in L_2(\Omega)$. Let \tilde{u}_H be the numerical solution of our proposed derivative-orthogonal wavelet multiscale method through numerically solving (2.21) in the finite-dimensional space $\tilde{V}_H := \text{span}(\tilde{\mathcal{B}}_H)$ with the basis $\tilde{\mathcal{B}}_H$ defined in (2.15). Then*

$$\|\sqrt{a}(u' - (\tilde{u}_H)')\|_{L_2(\Omega)} \leq CH \quad \text{with} \quad C := \frac{2}{\sqrt{a_{\min}}} \|f\|_{L_2(\Omega)}. \quad (2.28)$$

where H is the coarse mesh size such that $H = 2^{-n}$ for each integer $n \geq 2$.

Proof. Recall that (1.2) and (2.21) indicate that the exact solution $u \in H_0^1(\Omega)$ and the numerical solution $\tilde{u}_H \in \text{span}(\tilde{\mathcal{B}}_H) \subset H_0^1(\Omega)$ satisfy

$$\begin{aligned} \int_{\Omega} a u' v' dx &= \int_{\Omega} f v dx, & \text{for all } v \in H_0^1(\Omega), \\ \int_{\Omega} a(x) (\tilde{u}_H)' (\tilde{v}_H)' dx &= \int_{\Omega} f \tilde{v}_H dx, & \text{for all } \tilde{v}_H \in \text{span}(\tilde{\mathcal{B}}_H) \subset H_0^1(\Omega). \end{aligned}$$

Take $v = \tilde{v}_H \in \text{span}(\tilde{\mathcal{B}}_H)$ in the first identity. Then we have the Galerkin orthogonality:

$$\int_{\Omega} a(x) (u - \tilde{u}_H)' (\tilde{v}_H)' dx = 0, \quad \text{for all } \tilde{v}_H \in \text{span}(\tilde{\mathcal{B}}_H). \quad (2.29)$$

For any $\tilde{v}_H \in \text{span}(\tilde{\mathcal{B}}_H)$, we also have

$$\begin{aligned} \int_{\Omega} a(x) (u' - (\tilde{v}_H)')^2 dx &= \int_{\Omega} a(x) (u' - (\tilde{u}_H)' + (\tilde{u}_H)' - (\tilde{v}_H)')^2 dx, \\ &= \int_{\Omega} a(x) (u' - (\tilde{u}_H)')^2 dx + 2 \int_{\Omega} a(x) (u' - (\tilde{u}_H)') ((\tilde{u}_H)' - (\tilde{v}_H)') dx \\ &\quad + \int_{\Omega} a(x) ((\tilde{u}_H)' - (\tilde{v}_H)')^2 dx. \end{aligned} \quad (2.30)$$

Since $\tilde{u}_H - \tilde{v}_H \in \text{span}(\tilde{\mathcal{B}}_H)$, (2.29) implies

$$\begin{aligned} \int_{\Omega} a(x) (u' - (\tilde{v}_H)')^2 dx &= \int_{\Omega} a(x) (u' - (\tilde{u}_H)')^2 dx + \int_{\Omega} a(x) ((\tilde{u}_H)' - (\tilde{v}_H)')^2 dx, \\ &\geq \int_{\Omega} a(x) (u' - (\tilde{u}_H)')^2 dx. \end{aligned} \quad (2.31)$$

That is, we proved

$$\int_{\Omega} a(x) (u' - (\tilde{u}_H)')^2 dx \leq \int_{\Omega} a(x) (u' - (\tilde{v}_H)')^2 dx, \quad \text{for any } \tilde{v}_H \in \text{span}(\tilde{\mathcal{B}}_H). \quad (2.32)$$

On the other hand, we define

$$\xi_i = w_i \chi_{[\frac{i}{2^n}, \frac{i+1}{2^n})} \quad \text{and} \quad \eta_i = S'_i, \quad (2.33)$$

where $i = 0, \dots, 2^n - 1$, w_i and S'_i are defined in (2.10) and (2.13) respectively. Let

$$\xi = \sum_{i=0}^{2^n-1} \xi_i, \quad \eta = \sum_{i=0}^{2^n-1} \eta_i. \quad (2.34)$$

Then we conclude from (2.13) that

$$\xi + \eta = \frac{1}{a}, \quad \text{for all } x \in \Omega. \quad (2.35)$$

Furthermore, (2.26), (2.33), (2.34), Lemmas 2.3 and 2.4 together imply that

$$\xi \in \text{span}(\mathcal{B}'_H), \quad \eta \in \text{span}(\tilde{\mathcal{B}}'_H). \quad (2.36)$$

From the model problem (1.1), we have

$$-(au')' = f \implies a(x)u'(x) = - \int_0^x f(t)dt + K,$$

where K is a constant to be determined later. Define

$$F(x) := - \int_0^x f(t) dt, \quad x \in \Omega. \quad (2.37)$$

Note that we are considering the 1D problem, i.e., $\Omega = (0, 1)$. By our assumption $f \in L_2(\Omega)$, we must have $F \in H^1(\Omega) \subset C(\Omega)$ and $F(0) = 0$. Using the definition of the function F , we can rewrite the identity $a(x)u'(x) = - \int_0^x f(t)dt + K$ as

$$u'(x) = \frac{F(x) + K}{a(x)}. \quad (2.38)$$

Because $F \in H^1(\Omega) \subset C(\Omega)$, we have $au' \in C(\Omega)$. Furthermore, $u \in H_0^1(\Omega) \subset C(\Omega)$. We choose the constant K to be

$$K := \frac{- \int_0^1 F(t)/a(t)dt}{\int_0^1 1/a(t)dt}. \quad (2.39)$$

Consequently, we obtain from the above choice of the constant K that

$$\int_0^1 \frac{F(t) + K}{a(t)} dt = \int_0^1 \frac{F(t)}{a(t)} dt + K \int_0^1 \frac{1}{a(t)} dt = 0. \quad (2.40)$$

Now, (2.38)–(2.40) imply that the exact solution u of (1.1) can be written as

$$u(x) = \int_0^x \frac{F(t) + K}{a(t)} dt, \quad (2.41)$$

with

$$u(0) = \int_0^0 \frac{F(t) + K}{a(t)} dt = 0, \quad \text{and} \quad u(1) = \int_0^1 \frac{F(t) + K}{a(t)} dt = 0.$$

Define a piecewise constant function g on Ω by

$$g(x) = g_i, \quad \text{for } x \in \left[\frac{i}{2^n}, \frac{i+1}{2^n} \right), \quad i = 0, \dots, 2^n - 1 \quad \text{with} \quad g_i := \frac{\int_{\frac{i}{2^n}}^{\frac{i+1}{2^n}} \frac{F(x)+K}{a(x)} dx}{\int_{\frac{i}{2^n}}^{\frac{i+1}{2^n}} \frac{1}{a(x)} dx}. \quad (2.42)$$

By the definition of the function g in (2.42), we have

$$\|F + K - g\|_{L^2(\Omega)}^2 = \int_0^1 (F + K - g)^2 dx = \sum_{i=0}^{2^n-1} \int_{\frac{i}{2^n}}^{\frac{i+1}{2^n}} (F + K - g_i)^2 dx. \quad (2.43)$$

Note that both K and g_i are constant in $(\frac{i}{2^n}, \frac{i+1}{2^n})$. We observe from the definition of g_i in (2.42) that

$$\int_{\frac{i}{2^n}}^{\frac{i+1}{2^n}} \frac{F + K - g_i}{a} dx = \int_{\frac{i}{2^n}}^{\frac{i+1}{2^n}} \frac{F + K}{a} dx - g_i \int_{\frac{i}{2^n}}^{\frac{i+1}{2^n}} \frac{1}{a} dx = 0.$$

Since $F(x) + K - g_i$ is continuous on $(\frac{i}{2^n}, \frac{i+1}{2^n})$ and $a(x) > 0$ in Ω , the above identity implies that there must exist $x_0 \in (\frac{i}{2^n}, \frac{i+1}{2^n})$ such that

$$F(x_0) + K - g_i = 0. \quad (2.44)$$

Hence, by $x_0 \in (\frac{i}{2^n}, \frac{i+1}{2^n})$, we have

$$\int_{\frac{i}{2^n}}^{\frac{i+1}{2^n}} (F + K - g_i)^2 dx = \int_{\frac{i}{2^n}}^{x_0} (F + K - g_i)^2 dx + \int_{x_0}^{\frac{i+1}{2^n}} (F + K - g_i)^2 dx. \quad (2.45)$$

Note that $F \in H^1(\Omega) \subset C(\Omega)$. Using the integration by parts and (2.37), we deduce from (2.44) that

$$\begin{aligned} \int_{\frac{i}{2^n}}^{x_0} (F + K - g_i)^2 dx &= \int_{\frac{i}{2^n}}^{x_0} (F + K - g_i)^2 d(x - i/2^n) \\ &= (F + K - g_i)^2 \left(x - \frac{i}{2^n} \right) \Big|_{\frac{i}{2^n}}^{x_0} - 2 \int_{\frac{i}{2^n}}^{x_0} (x - i/2^n)(F + K - g_i)(-f(x)) dx, \\ &= 2 \int_{\frac{i}{2^n}}^{x_0} (x - i/2^n)(F + K - g_i) f dx \leq 2 \int_{\frac{i}{2^n}}^{x_0} |x - i/2^n| |(F + K - g_i) f| dx, \\ &\leq 2 \frac{1}{2^n} \int_{\frac{i}{2^n}}^{x_0} |(F + K - g_i) f| dx. \end{aligned} \quad (2.46)$$

Recall that $H = \frac{1}{2^n}$. Using the Cauchy-Schwarz inequality, (2.46) leads to

$$\left(\int_{\frac{i}{2^n}}^{x_0} (F + K - g_i)^2 dx \right)^2 \leq 4H^2 \left(\int_{\frac{i}{2^n}}^{x_0} (F + K - g_i)^2 dx \right) \left(\int_{\frac{i}{2^n}}^{x_0} f^2 dx \right), \quad (2.47)$$

from which we deduce that $\int_{\frac{i}{2^n}}^{x_0} (F + K - g_i)^2 dx \leq 4H^2 \int_{\frac{i}{2^n}}^{x_0} f^2 dx$. Similarly, we have $\int_{x_0}^{\frac{i+1}{2^n}} (F + K - g_i)^2 dx \leq 4H^2 \int_{x_0}^{\frac{i+1}{2^n}} f^2 dx$. Consequently, we conclude that

$$\int_{\frac{i}{2^n}}^{\frac{i+1}{2^n}} (F + K - g_i)^2 dx \leq 4H^2 \int_{\frac{i}{2^n}}^{x_0} f^2 dx + 4H^2 \int_{x_0}^{\frac{i+1}{2^n}} f^2 dx = 4H^2 \int_{\frac{i}{2^n}}^{\frac{i+1}{2^n}} f^2 dx.$$

According to (2.43) and the above inequality, we conclude that

$$\|F + K - g\|_{L_2(\Omega)}^2 \leq 4H^2 \|f\|_{L_2(\Omega)}^2. \quad (2.48)$$

Furthermore, (2.26), (2.42), Lemmas 2.3 and 2.4 together imply that

$$g \in \text{span}(\mathcal{B}'_H), \quad (2.49)$$

and by (2.42), we have

$$\int_0^1 \frac{g(x)}{a(x)} dx = \sum_{i=0}^{2^n-1} g_i \int_{\frac{i}{2^n}}^{\frac{i+1}{2^n}} \frac{1}{a(x)} dx = \sum_{i=0}^{2^n-1} \int_{\frac{i}{2^n}}^{\frac{i+1}{2^n}} \frac{F(x) + K}{a(x)} dx = \int_0^1 \frac{F(x) + K}{a(x)} dx.$$

By (2.40), we conclude from the above identity that

$$\int_0^1 \frac{g(x)}{a(x)} dx = 0. \quad (2.50)$$

Note that (2.35) holds. Define

$$w(x) := \int_0^x (\xi(t) + \eta(t))g(t) dt \stackrel{\text{by (2.35)}}{=} \int_0^x \frac{g(t)}{a(t)} dt. \quad (2.51)$$

Based on (2.26), (2.36), (2.49), Lemmas 2.3 and 2.4, it follows that

$$\frac{d}{dx} w(x) = \frac{g(x)}{a(x)} \in \text{span}(\tilde{\mathcal{B}}'_H).$$

Using the definition of $\tilde{\mathcal{B}}'_H$ in (2.26), we conclude from the above identity that

$$w(x) \in \text{span}(\tilde{\mathcal{B}}_H \cup \{x + b, 1\}), \quad (2.52)$$

where b is a constant. So (2.19) implies that

$$w(x) = \sum_{i=1}^M d_i \varphi_i(x) + d_{M+1}(x + b) + d_{M+2}, \quad (2.53)$$

where each d_i is a constant. By (2.50) and (2.51),

$$w(0) = w(1) = 0. \quad (2.54)$$

So, (2.16), (2.53) and (2.54) yield

$$d_{M+1}(0 + b) + d_{M+2} = 0, \quad d_{M+1}(1 + b) + d_{M+2} = 0 \implies d_{M+1} = d_{M+2} = 0.$$

Consequently, we conclude from (2.53) that $w(x) = \sum_{i=1}^M d_i \varphi_i(x)$, that is,

$$w \in \text{span}(\tilde{\mathcal{B}}_H) \subset H_0^1(\Omega). \quad (2.55)$$

Using (2.38) and (2.51), due to $\frac{1}{a(x)} \leq \frac{1}{a_{\min}}$ for all $x \in \Omega$, we have

$$\begin{aligned} \int_{\Omega} a(x) (u' - w')^2 dx &= \int_{\Omega} a(x) \left(\frac{F + K}{a} - \frac{g}{a} \right)^2 dx = \int_{\Omega} \frac{1}{a(x)} (F + K - g)^2 dx, \\ &\leq \frac{1}{a_{\min}} \int_{\Omega} (F + K - g)^2 dx \leq \frac{4}{a_{\min}} H^2 \|f\|_{L_2(\Omega)}^2, \end{aligned} \quad (2.56)$$

where we used (2.48) in the last inequality. From (2.32) and (2.55), we deduce from the fact $w \in \text{span}(\tilde{\mathcal{B}}_H)$ that

$$\int_{\Omega} a(x) (u' - (\tilde{u}_H)')^2 dx \leq \int_{\Omega} a(x) (u' - (w)')^2 dx \leq C^2 H^2, \quad (2.57)$$

where we used (2.56) in the last inequality and $C := \frac{2}{\sqrt{a_{\min}}} \|f\|_{L_2(\Omega)}$. \square

Utilizing (2.28) in Theorem 2.5 and the well-known Aubin–Nitsche argument, we now theoretically prove that the L_2 norm of the error of our proposed method achieves the second-order convergence rate for any coarse mesh size H in the following Theorem 2.6.

Theorem 2.6. *Define $a_{\max} := \sup_{x \in \Omega} a(x)$ and $a_{\min} := \inf_{x \in \Omega} a(x)$. Let u be the exact solution of the model problem (1.1) under the assumptions that $0 < a_{\min} \leq a \leq a_{\max} < \infty$ and $f \in L_2(\Omega)$. Let \tilde{u}_H be the numerical solution of our proposed derivative-orthogonal wavelet multiscale method through numerically solving (2.21) in the finite-dimensional space $\tilde{V}_H := \text{span}(\tilde{\mathcal{B}}_H)$ with the basis $\tilde{\mathcal{B}}_H$ defined in (2.15). Then*

$$\|u - \tilde{u}_H\|_{L_2(\Omega)} \leq CH^2 \quad \text{with} \quad C := \frac{4}{a_{\min}} \|f\|_{L_2(\Omega)}, \quad (2.58)$$

where H is the coarse mesh size such that $H = 2^{-n}$ for each integer $n \geq 2$.

Proof. We use the Aubin–Nitsche argument. Let $z \in H_0^1(\Omega)$ be the solution to

$$-\nabla \cdot (a \nabla z) = u - \tilde{u}_H, \quad (2.59)$$

with the boundary conditions $z(0) = z(1) = 0$. Then

$$\|u - \tilde{u}_H\|_{L_2(\Omega)}^2 = \int_{\Omega} (u - \tilde{u}_H)^2 dx = \int_{\Omega} -\nabla \cdot (a \nabla z) (u - \tilde{u}_H) dx = \int_{\Omega} a(x) z' (u - \tilde{u}_H)' dx.$$

Let $\tilde{z}_H \in \text{span}(\tilde{\mathcal{B}}_H) \subseteq H_0^1(\Omega)$ be the unique solution to $\int_{\Omega} a \nabla \tilde{z}_H \cdot \nabla \tilde{v}_H dx = \int_{\Omega} (u - \tilde{u}_H) \tilde{v}_H dx$ for all $\tilde{v}_H \in \text{span}(\tilde{\mathcal{B}}_H)$. Applying the Galerkin orthogonality in (2.29) with $\tilde{v}_H = \tilde{z}_H \in \text{span}(\tilde{\mathcal{B}}_H)$ and using the Cauchy-Schwarz inequality, we derive from the above identity that

$$\begin{aligned} \|u - \tilde{u}_H\|_{L_2(\Omega)}^2 &= \int_{\Omega} a(x) z' (u - \tilde{u}_H)' dx = \int_{\Omega} a(x) (z - \tilde{z}_H)' (u - \tilde{u}_H)' dx, \\ &\leq \|\sqrt{a}(z - \tilde{z}_H)'\|_{L_2(\Omega)} \|\sqrt{a}(u - \tilde{u}_H)'\|_{L_2(\Omega)} \leq \|\sqrt{a}(z - \tilde{z}_H)'\|_{L_2(\Omega)} \frac{2}{\sqrt{a_{\min}}} \|f\|_{L_2(\Omega)} H, \end{aligned} \quad (2.60)$$

where we used the inequality (2.28) of Theorem 2.5 in the last inequality. Note that $u - \tilde{u}_H \in L_2(\Omega)$. Applying (2.28) of Theorem 2.5 and (2.59), we must have

$$\|\sqrt{a}(z - \tilde{z}_H)'\|_{L_2(\Omega)} \leq \frac{2}{\sqrt{a_{\min}}} \|u - \tilde{u}_H\|_{L_2(\Omega)} H. \quad (2.61)$$

Now, we conclude from (2.60) and (2.61) that

$$\|u - \tilde{u}_H\|_{L_2(\Omega)}^2 \leq \frac{2}{\sqrt{a_{\min}}} \|u - \tilde{u}_H\|_{L_2(\Omega)} H \frac{2}{\sqrt{a_{\min}}} \|f\|_{L_2(\Omega)} H = \frac{4}{a_{\min}} \|f\|_{L_2(\Omega)} \|u - \tilde{u}_H\|_{L_2(\Omega)} H^2,$$

from which we obtain $\|u - \tilde{u}_H\|_{L_2(\Omega)} \leq \frac{4}{a_{\min}} \|f\|_{L_2(\Omega)} H^2$. \square

Finally, we introduce the following Lemma 2.7 to show the interpolation property that $\tilde{u}_H(\frac{i}{2^n}) = u(\frac{i}{2^n})$, for $i = 0, 1, \dots, 2^n$, where u is the exact solution of (1.1), \tilde{u}_H is the numerical solution of our proposed derivative-orthogonal wavelet multiscale method, and H is the coarse mesh size such that $H = 2^{-n}$ for each integer $n \geq 2$.

Lemma 2.7. *Define the continuous piecewise linear interpolations*

$$\ell_i := \begin{cases} 2^n(x - \frac{i}{2^n}), & x \in [\frac{i}{2^n}, \frac{i+1}{2^n}), \\ 2^n(-x + \frac{i+2}{2^n}), & x \in [\frac{i+1}{2^n}, \frac{i+2}{2^n}), \\ 0, & \text{else,} \end{cases} \quad (2.62)$$

where $i = 0, 1, \dots, 2^n - 2$ and n is an integer with $n \geq 2$. Then

$$\text{span}\{\ell_i : i = 0, 1, \dots, 2^n - 2\} = V_H := \text{span}(\mathcal{B}_H), \quad (2.63)$$

where \mathcal{B}_H is defined in (2.4).

Proof. (2.63) is a direct consequence due to the way we construct the wavelet basis \mathcal{B}_H of V_H in (2.4). See [14, 15] for details on wavelets and their refinable structure. \square

Now, by Lemma 2.7, we can prove the following result on the interpolation property.

Theorem 2.8. *Define $a_{\max} := \sup_{x \in \Omega} a(x)$ and $a_{\min} := \inf_{x \in \Omega} a(x)$. Let u be the exact solution of the model problem (1.1) under the assumptions that $0 < a_{\min} \leq a \leq a_{\max} < \infty$ and $f \in L_2(\Omega)$. Let \tilde{u}_H be the numerical solution of our proposed derivative-orthogonal wavelet multiscale method through numerically solving (2.21) in the finite-dimensional space $\tilde{V}_H := \text{span}(\tilde{\mathcal{B}}_H)$ with the basis $\tilde{\mathcal{B}}_H$ defined in (2.15). Then*

$$\tilde{u}_H \left(\frac{i}{2^n} \right) = u \left(\frac{i}{2^n} \right), \quad \text{for } i = 0, 1, \dots, 2^n, \quad (2.64)$$

where H is the coarse mesh size such that $H = 2^{-n}$ for each integer $n \geq 2$.

Proof. We define

$$\beta_i := \frac{S_i}{w_i} - \frac{S_{i+1}}{w_{i+1}}, \quad \text{for } i = 0, 1, \dots, 2^n - 2, \quad (2.65)$$

where S_i is defined in (2.9) and each constant w_i is defined in (2.10). By (2.10), each constant $w_i > 0$. (2.9) and (2.10) also imply that

$$S_i = 0, \quad \text{and} \quad w_i = \frac{1}{\mathbf{k}_i}, \quad \text{if } a \text{ is equal to a positive constant } \mathbf{k}_i \text{ in } \left(\frac{i}{2^n}, \frac{i+1}{2^n} \right). \quad (2.66)$$

From (2.13) and (2.65), it follows that:

$$(\beta_i)' = \begin{cases} \frac{1}{w_i a} - 1, & x \in [\frac{i}{2^n}, \frac{i+1}{2^n}), \\ \frac{-1}{w_{i+1} a} + 1, & x \in [\frac{i+1}{2^n}, \frac{i+2}{2^n}), \\ 0, & \text{else,} \end{cases} \quad (2.67)$$

where $i = 0, 1, \dots, 2^n - 2$. Clearly, if a is equal to a positive constant \mathbf{k}_i in $(\frac{i}{2^n}, \frac{i+1}{2^n})$, then (2.66) yields

$$\beta_i = -\frac{S_{i+1}}{w_{i+1}}, \quad (\beta_i)' = \begin{cases} \frac{-1}{w_{i+1} a} + 1, & x \in [\frac{i+1}{2^n}, \frac{i+2}{2^n}), \\ 0, & \text{else.} \end{cases} \quad (2.68)$$

By the definition of $\tilde{\mathcal{B}}_H$ in (2.15) and the definition of β_i in (2.65), we identify that

$$\beta_i \in \text{span}(\tilde{\mathcal{B}}_H), \quad \text{for } i = 0, 1, \dots, 2^n - 2. \quad (2.69)$$

Define ℓ_i as in (2.62) with $i = 0, 1, \dots, 2^n - 2$. It is clear that

$$(\ell_i)' = \begin{cases} 2^n, & x \in [\frac{i}{2^n}, \frac{i+1}{2^n}), \\ -2^n, & x \in [\frac{i+1}{2^n}, \frac{i+2}{2^n}), \\ 0, & \text{else.} \end{cases} \quad (2.70)$$

By (2.63) in Lemma 2.7, definitions of \mathcal{B}_H and $\tilde{\mathcal{B}}_H$ in (2.4) and (2.15), we observe

$$\ell_i \in \text{span}(\mathcal{B}_H) \subset \text{span}(\tilde{\mathcal{B}}_H), \quad \text{for } i = 0, 1, \dots, 2^n - 2. \quad (2.71)$$

Define the error

$$E := u - \tilde{u}_H. \quad (2.72)$$

Then, (2.29) implies

$$\int_{\Omega} a(x)E'(\tilde{v}_H)' dx = \int_{\Omega} a(x)(u - \tilde{u}_H)'(\tilde{v}_H)' dx = 0, \quad \text{for all } \tilde{v}_H \in \text{span}(\tilde{\mathcal{B}}_H). \quad (2.73)$$

We deduce from (2.70), (2.71), and (2.73) that

$$0 = \frac{1}{2^n} \int_{\Omega} a(x)E'(x)(\ell_i(x))' dx = \int_{\frac{i}{2^n}}^{\frac{i+1}{2^n}} a(x)E'(x) dx + \int_{\frac{i+1}{2^n}}^{\frac{i+2}{2^n}} a(x)E'(x)(-1) dx. \quad (2.74)$$

We claim that

$$0 = \frac{1}{w_i} \int_{\frac{i}{2^n}}^{\frac{i+1}{2^n}} E' dx - \frac{1}{w_{i+1}} \int_{\frac{i+1}{2^n}}^{\frac{i+2}{2^n}} E' dx, \quad (2.75)$$

where each constant w_i is defined in (2.10). We prove (2.75) by following (2.76)–(2.79) in the following 3 cases.

Case 1. If a is not equal to a positive constant k_i in each $(\frac{i}{2^n}, \frac{i+1}{2^n})$ with $i = 0, 1, \dots, 2^n - 2$. We conclude from (2.67), (2.69), and (2.73) that

$$\begin{aligned} 0 &= \int_{\Omega} aE'(\beta_i)' dx = \int_{\frac{i}{2^n}}^{\frac{i+1}{2^n}} aE' \left(\frac{1}{w_i a} - 1 \right) dx + \int_{\frac{i+1}{2^n}}^{\frac{i+2}{2^n}} aE' \left(\frac{-1}{w_{i+1} a} + 1 \right) dx, \\ &= \frac{1}{w_i} \int_{\frac{i}{2^n}}^{\frac{i+1}{2^n}} E' dx - \frac{1}{w_{i+1}} \int_{\frac{i+1}{2^n}}^{\frac{i+2}{2^n}} E' dx - \int_{\frac{i}{2^n}}^{\frac{i+1}{2^n}} aE' dx + \int_{\frac{i+1}{2^n}}^{\frac{i+2}{2^n}} aE' dx. \end{aligned} \quad (2.76)$$

Then (2.76) and (2.74) lead to (2.75).

Case 2. If $a = k_i$ for $x \in (\frac{i}{2^n}, \frac{i+1}{2^n})$, then (2.68) implies

$$0 = \int_{\Omega} aE'(\beta_i)' dx = \int_{\frac{i+1}{2^n}}^{\frac{i+2}{2^n}} aE' \left(\frac{-1}{w_{i+1} a} + 1 \right) dx = -\frac{1}{w_{i+1}} \int_{\frac{i+1}{2^n}}^{\frac{i+2}{2^n}} E' dx + \int_{\frac{i+1}{2^n}}^{\frac{i+2}{2^n}} aE' dx. \quad (2.77)$$

Now, (2.74) indicates

$$0 = \int_{\frac{i}{2^n}}^{\frac{i+1}{2^n}} aE' dx - \int_{\frac{i+1}{2^n}}^{\frac{i+2}{2^n}} aE' dx = k_i \int_{\frac{i}{2^n}}^{\frac{i+1}{2^n}} E' dx - \int_{\frac{i+1}{2^n}}^{\frac{i+2}{2^n}} aE' dx. \quad (2.78)$$

(2.77) and (2.78) together with $k_i = \frac{1}{w_i}$ in (2.66) leads to (2.75).

Case 3. If a is a positive constant function k for $x \in (0, 1)$, then (2.10) suggests

$$w_0 = w_1 = \dots = w_{2^n-1} = \frac{1}{k}.$$

By (2.74),

$$0 = k \int_{\frac{i}{2^n}}^{\frac{i+1}{2^n}} E' dx - k \int_{\frac{i+1}{2^n}}^{\frac{i+2}{2^n}} E' dx = \frac{1}{w_i} \int_{\frac{i}{2^n}}^{\frac{i+1}{2^n}} E' dx - \frac{1}{w_{i+1}} \int_{\frac{i+1}{2^n}}^{\frac{i+2}{2^n}} E' dx. \quad (2.79)$$

Thus, (2.75) is true for any constant $a > 0$ on Ω .

Since $E = u - \tilde{u}_H$ is continuous in Ω , we have

$$\int_{\frac{i}{2^n}}^{\frac{i+1}{2^n}} E' dx = E \left(\frac{i+1}{2^n} \right) - E \left(\frac{i}{2^n} \right), \quad \text{and} \quad \int_{\frac{i+1}{2^n}}^{\frac{i+2}{2^n}} E' dx = E \left(\frac{i+2}{2^n} \right) - E \left(\frac{i+1}{2^n} \right).$$

Now, (2.75) yields

$$-\frac{1}{w_i}E\left(\frac{i}{2^n}\right) + \left(\frac{1}{w_i} + \frac{1}{w_{i+1}}\right)E\left(\frac{i+1}{2^n}\right) - \frac{1}{w_{i+1}}E\left(\frac{i+2}{2^n}\right) = 0, \quad (2.80)$$

for $i = 0, 1, \dots, 2^n - 2$. We define

$$\vec{E} := \left(E(0), E\left(\frac{1}{2^n}\right), E\left(\frac{2}{2^n}\right), \dots, E\left(\frac{2^n-1}{2^n}\right), E(1)\right)^T. \quad (2.81)$$

By the boundary condition $u(0) = u(1) = 0$, it is obvious that $E(0) = E(1) = 0$. So (2.80) and (2.81) indicate

$$A\vec{E} = \vec{0}, \quad (2.82)$$

where

$$A = \begin{pmatrix} 1 & 0 & 0 & 0 & 0 & 0 & \dots & 0 & 0 \\ -\frac{1}{w_0} & \frac{1}{w_0} + \frac{1}{w_1} & -\frac{1}{w_1} & 0 & 0 & 0 & \dots & 0 & 0 \\ 0 & -\frac{1}{w_1} & \frac{1}{w_1} + \frac{1}{w_2} & -\frac{1}{w_2} & 0 & 0 & \dots & 0 & 0 \\ 0 & 0 & -\frac{1}{w_2} & \frac{1}{w_2} + \frac{1}{w_3} & -\frac{1}{w_3} & 0 & \dots & 0 & 0 \\ 0 & 0 & 0 & -\frac{1}{w_3} & \frac{1}{w_3} + \frac{1}{w_4} & -\frac{1}{w_4} & \ddots & 0 & 0 \\ \vdots & \vdots & \vdots & \ddots & \ddots & \ddots & \ddots & 0 & 0 \\ 0 & 0 & 0 & \dots & 0 & -\frac{1}{w_{2^n-3}} & \frac{1}{w_{2^n-3}} + \frac{1}{w_{2^n-2}} & -\frac{1}{w_{2^n-2}} & 0 \\ 0 & 0 & 0 & 0 & \dots & 0 & -\frac{1}{w_{2^n-2}} & \frac{1}{w_{2^n-2}} + \frac{1}{w_{2^n-1}} & -\frac{1}{w_{2^n-1}} \\ 0 & 0 & 0 & 0 & 0 & \dots & 0 & 0 & 1 \end{pmatrix}.$$

Since the above A is a $(2^n + 1) \times (2^n + 1)$ M-matrix, we can say that A is invertible. Now (2.82) leads to $\vec{E} = \vec{0}$. From (2.72) and (2.81), we observe that

$$\tilde{u}_H\left(\frac{i}{2^n}\right) = u\left(\frac{i}{2^n}\right), \quad \text{where } i = 0, 1, \dots, 2^n, \quad \text{and } H = \frac{1}{2^n}. \quad (2.83)$$

Thus, (2.64) is proved. \square

3. NUMERICAL EXPERIMENTS

Recall that $\Omega = (0, 1)$, $H = \frac{1}{2^n}$ for every integer $n \geq 2$, u is the exact solution of the model problem (1.1), \tilde{u}_H is the numerical solution of our proposed derivative-orthogonal wavelet multiscale method through solving (2.21) by using the basis $\tilde{\mathcal{B}}_H$ in (2.15). We shall measure errors in l_2 and l_∞ norms on an extremely fine mesh $\frac{1}{N}\mathbb{Z} \cap \bar{\Omega}$ with very large integers N . That is, we define

$$x_i = i/N, \quad i = 0, \dots, N, \quad \text{for very large integers } N. \quad (3.1)$$

For all our numerical examples, we shall use either $N = 2^{14}$ or 2^{15} . To verify the convergence rate, we define the following l_2 and l_∞ norms if the exact solution u is available

$$\begin{aligned} \frac{\|\tilde{u}_H - u\|_2}{\|u\|_2} &:= \sqrt{\frac{\sum_{i=0}^N |\tilde{u}_H(x_i) - u(x_i)|^2}{\sum_{i=0}^N |u(x_i)|^2}}, & \frac{\|\tilde{u}'_H - u'\|_2}{\|u'\|_2} &:= \sqrt{\frac{\sum_{i=0}^N |\tilde{u}'_H(x_i) - u'(x_i)|^2}{\sum_{i=0}^N |u'(x_i)|^2}}, \\ \frac{\|a\tilde{u}'_H - au'\|_2}{\|au'\|_2} &:= \sqrt{\frac{\sum_{i=0}^N |a(x_i)\tilde{u}'_H(x_i) - a(x_i)u'(x_i)|^2}{\sum_{i=0}^N |a(x_i)u'(x_i)|^2}}, \end{aligned} \quad (3.2)$$

for measuring the errors in l_2 norms, and

$$\begin{aligned} \|\tilde{u}_H - u\|_\infty &:= \max_{0 \leq i \leq N} |\tilde{u}_H(x_i) - u(x_i)|, & \|\tilde{u}'_H - u'\|_\infty &:= \max_{0 \leq i \leq N} |\tilde{u}'_H(x_i) - u'(x_i)|, \\ \|a\tilde{u}'_H - au'\|_\infty &:= \max_{0 \leq i \leq N} |a(x_i)\tilde{u}'_H(x_i) - a(x_i)u'(x_i)|, \end{aligned} \quad (3.3)$$

for measuring the errors in l_∞ norms.

If the exact solution u is not available, we replace u by $\tilde{u}_{H/2}$ in (3.2)–(3.3) to define following l_2 and l_∞ norms

$$\begin{aligned} \frac{\|\tilde{u}_H - \tilde{u}_{H/2}\|_2}{\|\tilde{u}_{H/2}\|_2}, & \quad \frac{\|\tilde{u}'_H - \tilde{u}'_{H/2}\|_2}{\|\tilde{u}'_{H/2}\|_2}, & \quad \frac{\|a\tilde{u}'_H - a\tilde{u}'_{H/2}\|_2}{\|a\tilde{u}'_{H/2}\|_2}, & \quad l_2 \text{ norms,} \\ \|\tilde{u}_H - \tilde{u}_{H/2}\|_\infty, & \quad \|\tilde{u}'_H - \tilde{u}'_{H/2}\|_\infty, & \quad \|a\tilde{u}'_H - a\tilde{u}'_{H/2}\|_\infty, & \quad l_\infty \text{ norms.} \end{aligned}$$

To highlight benefits of our proposed multiscale method (2.21), in Examples 1 to 3, we shall compare the l_2 and l_∞ norms of errors of the above numerical solution \tilde{u}_H with these of the linear finite element solution $u_{H/2} \in \text{span}\{\ell_i : i = 0, \dots, 2^{n+1} - 2\}$ satisfying

$$\int_{\Omega} a \nabla u_{H/2} \cdot \nabla v = \int_{\Omega} f v, \quad \text{for all } v \in \{\ell_i : i = 0, \dots, 2^{n+1} - 2\}, \quad (3.4)$$

where $\{\ell_i : i = 0, \dots, 2^{n+1} - 2\}$ is obtained by replacing n with $n + 1$ in (2.62). Precisely, we present the errors in Table 3 for Example 1, Table 6 for Example 2, and Table 9 for Example 3 by replacing the above numerical solution \tilde{u}_H with the solution $u_{H/2}$ in (3.2) and (3.3). By (2.63), $\text{span}\{\ell_i : i = 0, 1, \dots, 2^{n+1} - 2\} = \text{span}(\mathcal{B}_{H/2})$. Due to $H = 2^{-n}$ and the refinability structure of \mathcal{B}_H , we observe ([14,15]) that $\mathcal{B}_{H/2} \subset \tilde{\mathcal{B}}_{H/2}$, while the three bases $\{\ell_i : i = 0, 1, \dots, 2^{n+1} - 2\}$, $\mathcal{B}_{H/2}$ and $\tilde{\mathcal{B}}_H$ have the same cardinality $2^{n+1} - 1$. In Table 1–Table 15 of Example 1–Example 6, κ is the condition number of the stiffness matrix of our proposed derivative-orthogonal wavelet multiscale method or the standard finite element method (FEM). We test 6 numerical examples with $\Omega = (0, 1)$ in this section.

3.1. The exact solution u is available.

Example 1. Consider $f(x) = 1000x$ and a continuous diffusion coefficient $a(x) = \frac{1}{1.05 + \sin(2^9 \pi x)}$ having the high-frequency oscillation. Then the exact solution u of (1.1) can be expressed as

$$u(x) = 1000 \left(-\frac{1.05x^3}{6} + \frac{c_1 \cos(2^9 \pi x)}{2^9 \pi} + \frac{\cos(2^9 \pi x)}{2^{10} \pi} x^2 - \frac{\cos(2^9 \pi x)}{(2^9 \pi)^3} - \frac{\sin(2^9 \pi x)}{2^9 \pi} x - 1.05c_1 x + c_2 \right),$$

where

$$\begin{aligned} c_1 &= \frac{1.05(2^9 \pi)^3 - 3 \cos(2^9 \pi)(2^9 \pi)^2 + 6 \sin(2^9 \pi)(2^9 \pi) + 6 \cos(2^9 \pi) - 6}{6(2^9 \pi)^2(-1.05(2^9 \pi) + \cos(2^9 \pi) - 1)}, \\ c_2 &= \frac{-1.05(2^9 \pi)^2 + 3 \cos(2^9 \pi)(2^9 \pi) - 6 \sin(2^9 \pi) - 6.3}{6(2^9 \pi)^2(-1.05(2^9 \pi) + \cos(2^9 \pi) - 1)}. \end{aligned}$$

The results on numerical solutions \tilde{u}_H and $u_{H/2}$ are presented in Tables 1 to 3 and Fig. 6.

TABLE 1. Performance of the l_2 norm of the errors in Example 1 of our proposed derivative-orthogonal wavelet multiscale method on the uniform Cartesian mesh H . Note that $N = 2^{14}$ in (3.1) for estimating the l_2 norm.

H	$\frac{\ \tilde{u}_H - u\ _2}{\ u\ _2}$	order	$\frac{\ \tilde{u}'_H - u'\ _2}{\ u'\ _2}$	order	$\frac{\ a\tilde{u}'_H - au'\ _2}{\ au'\ _2}$	order	κ	$\frac{a_{\max}}{a_{\min}}$
1/2	2.7782E-01		5.4501E-01		5.4490E-01		11.64	41
1/2 ²	7.1084E-02	1.97	2.7783E-01	0.97	2.7779E-01	0.97	11.64	41
1/2 ³	1.7870E-02	1.99	1.3955E-01	0.99	1.3957E-01	0.99	11.64	41
1/2 ⁴	4.4716E-03	2.00	6.9793E-02	1.00	6.9889E-02	1.00	11.64	41
1/2 ⁵	1.1162E-03	2.00	3.4779E-02	1.00	3.5001E-02	1.00	11.64	41
1/2 ⁶	2.7680E-04	2.01	1.7133E-02	1.02	1.7593E-02	0.99	11.64	41

TABLE 2. Performance of the l_∞ norm of the error in Example 1 of our proposed derivative-orthogonal wavelet multiscale method on the uniform Cartesian mesh H . Note that $N = 2^{14}$ in (3.1) for estimating the l_∞ norm.

H	$\ \tilde{u}_H - u\ _\infty$	order	$\ \tilde{u}'_H - u'\ _\infty$	order	$\ a\tilde{u}'_H - au'\ _\infty$	order	κ	$\frac{a_{\max}}{a_{\min}}$
$1/2$	2.4665E+01		4.2219E+02		2.0878E+02		11.64	41
$1/2^2$	7.1769E+00	1.78	2.3019E+02	0.88	1.1510E+02	0.86	11.64	41
$1/2^3$	1.9214E+00	1.90	1.1817E+02	0.96	6.0451E+01	0.93	11.64	41
$1/2^4$	4.9642E-01	1.95	5.8158E+01	1.02	3.1656E+01	0.93	11.64	41
$1/2^5$	1.2618E-01	1.98	2.8029E+01	1.05	1.6988E+01	0.90	11.64	41
$1/2^6$	3.1864E-02	1.99	1.2546E+01	1.16	9.4095E+00	0.85	11.64	41

TABLE 3. Performance of l_2 and l_∞ norms of the error in Example 1 of the standard second-order FEM on the uniform Cartesian mesh H . Note that $N = 2^{14}$ in (3.1) for estimating l_2 and l_∞ norms.

H	$\ u_{H/2} - u\ _2$	$\ u'_{H/2} - u'\ _2$	$\ au'_{H/2} - au'\ _2$	$\ u_{H/2} - u\ _\infty$	$\ u'_{H/2} - u'\ _\infty$	$\ au'_{H/2} - au'\ _\infty$	κ	$\frac{a_{\max}}{a_{\min}}$
	$\ u\ _2$	$\ u'\ _2$	$\ au'\ _2$					
$1/2$	7.1E-01	8.2E-01	1.5E+00	4.8E+01	6.1E+02	1.3E+03	5.8E+00	41
$1/2^2$	7.0E-01	8.1E-01	1.5E+00	4.7E+01	5.9E+02	1.5E+03	2.5E+01	41
$1/2^3$	7.0E-01	8.0E-01	1.5E+00	4.7E+01	5.8E+02	1.7E+03	1.0E+02	41
$1/2^4$	6.9E-01	8.0E-01	1.5E+00	4.7E+01	5.8E+02	1.7E+03	4.1E+02	41
$1/2^5$	6.9E-01	8.0E-01	1.5E+00	4.7E+01	5.7E+02	1.8E+03	1.7E+03	41
$1/2^6$	6.9E-01	8.0E-01	1.5E+00	4.7E+01	5.7E+02	1.8E+03	6.6E+03	41

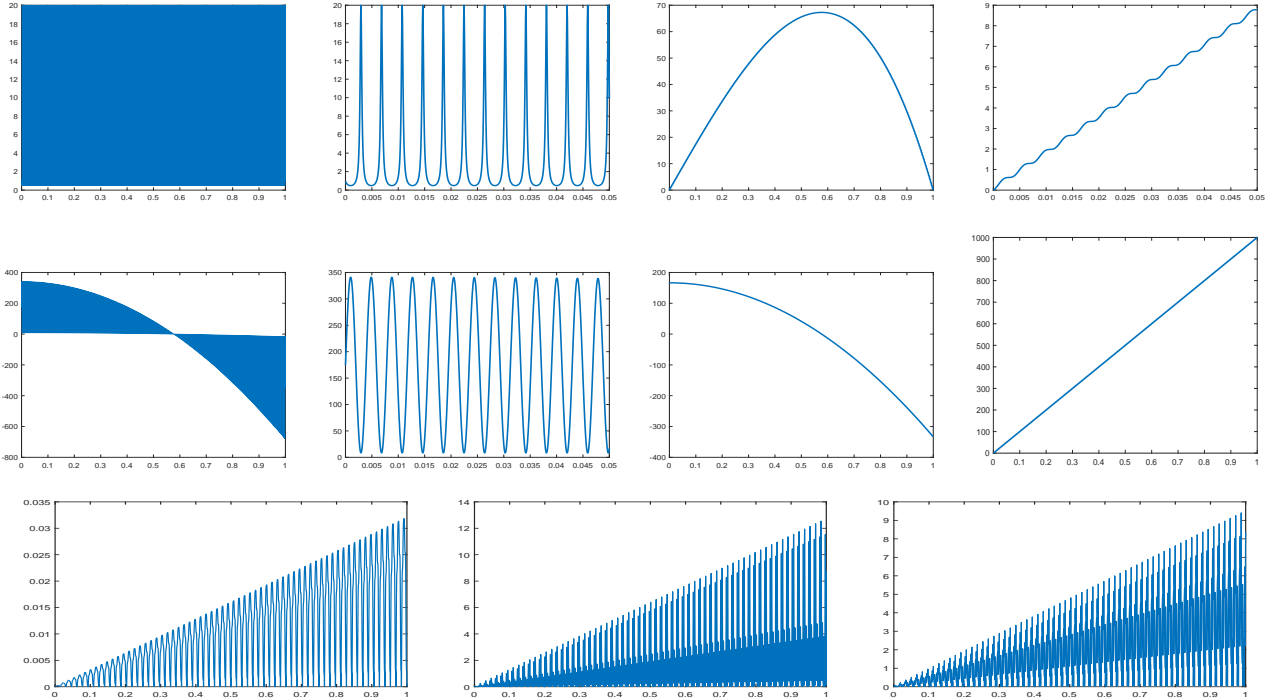


FIGURE 6. Example 1: The top row: a in $[0,1]$ (first panel), a in $[0,0.05]$ (second panel), u in $[0,1]$ (third panel), and u in $[0,0.05]$ (fourth panel). The middle row: u' in $[0,1]$ (first panel), u' in $[0,0.05]$ (second panel), au' in $[0,1]$ (third panel), and f in $[0,1]$ (fourth panel). The bottom row: $|\tilde{u}_H - u|$ (first panel), $|\tilde{u}'_H - u'|$ (second panel), and $|a\tilde{u}'_H - au'|$ (third panel) in $[0,1]$ with $H = \frac{1}{2^6}$ at all $x_i = i/N$ for $i = 0, \dots, N$ with $N = 2^{14}$ in (3.1).

Example 2. Consider $f(x) = x$ and a diffusion discontinuous coefficient with high-contrast jumps below

$$a(x) = 10^4 \chi_{[\frac{i-1}{2^8}, \frac{i}{2^8})} + 10^{-4} \chi_{[\frac{i}{2^8}, \frac{i+1}{2^8})}, \quad \text{with } i = 1, 3, 5, \dots, 2^8 - 1.$$

Then the exact solution u of (1.1) can be expressed as

$$u(x) = -\frac{1}{6} c_{i,3} x^3 + c_{i,1} x + c_{i,0} \quad \text{for } x \in \left[\frac{i-1}{2^8}, \frac{i}{2^8} \right] \quad \text{with } i = 1, 2, 3, \dots, 2^8,$$

where

$$c_{i,3} = \begin{cases} 10^{-4}, & \text{if } i \text{ is odd,} \\ 10^4, & \text{if } i \text{ is even,} \end{cases}$$

and the constants $c_{i,1}, c_{i,0}$ can be uniquely determined by imposing the continuity of u and au' at $x = \frac{i-1}{2^8}$ for $i = 2, 3, 4, \dots, 2^8$, along with the boundary condition $u(0) = u(1) = 0$. The results on numerical solutions \tilde{u}_H and $u_{H/2}$ are presented in Tables 4 to 6 and Fig. 7.

TABLE 4. Performance of the l_2 norm of the error in Example 2 of our proposed derivative-orthogonal wavelet multiscale method on the uniform Cartesian mesh H . Note that $N = 2^{14}$ in (3.1) for estimating the l_2 norm.

H	$\frac{\ \tilde{u}_H - u\ _2}{\ u\ _2}$	order	$\frac{\ \tilde{u}'_H - u'\ _2}{\ u'\ _2}$	order	$\frac{\ a\tilde{u}'_H - au'\ _2}{\ au'\ _2}$	order	κ	$\frac{a_{\max}}{a_{\min}}$
1/2	2.7754E-01		5.4457E-01		5.4483E-01		1.00E+08	1.00E+08
1/2 ²	7.0993E-02	1.97	2.7751E-01	0.97	2.7767E-01	0.97	1.00E+08	1.00E+08
1/2 ³	1.7837E-02	1.99	1.3926E-01	0.99	1.3934E-01	0.99	1.00E+08	1.00E+08
1/2 ⁴	4.4544E-03	2.00	6.9403E-02	1.00	6.9445E-02	1.00	1.00E+08	1.00E+08
1/2 ⁵	1.1021E-03	2.01	3.4087E-02	1.03	3.4109E-02	1.03	1.00E+08	1.00E+08
1/2 ⁶	2.6042E-04	2.08	1.5737E-02	1.12	1.5747E-02	1.12	1.00E+08	1.00E+08

TABLE 5. Performance of the l_∞ norm of the error in Example 2 of our proposed derivative-orthogonal wavelet multiscale method on the uniform Cartesian mesh H . Note that $N = 2^{14}$ in (3.1) for estimating the l_∞ norm.

H	$\ \tilde{u}_H - u\ _\infty$	order	$\ \tilde{u}'_H - u'\ _\infty$	order	$\ a\tilde{u}'_H - au'\ _\infty$	order	κ	$\frac{a_{\max}}{a_{\min}}$
1/2	1.1784E+02		2.0687E+03		2.0687E-01		1.00E+08	1.00E+08
1/2 ²	3.4260E+01	1.78	1.1287E+03	0.87	1.1287E-01	0.87	1.00E+08	1.00E+08
1/2 ³	9.1744E+00	1.90	5.8065E+02	0.96	5.8065E-02	0.96	1.00E+08	1.00E+08
1/2 ⁴	2.3699E+00	1.95	2.8707E+02	1.02	2.8707E-02	1.02	1.00E+08	1.00E+08
1/2 ⁵	6.0201E-01	1.98	1.3540E+02	1.08	1.3540E-02	1.08	1.00E+08	1.00E+08
1/2 ⁶	1.5169E-01	1.99	5.8340E+01	1.21	5.8340E-03	1.21	1.00E+08	1.00E+08

TABLE 6. Performance of l_2 and l_∞ norms of the error in Example 2 of the standard second-order FEM on the uniform Cartesian mesh H . Note that $N = 2^{14}$ in (3.1) for estimating l_2 and l_∞ norms.

H	$\frac{\ u_{H/2} - u\ _2}{\ u\ _2}$	$\frac{\ u'_{H/2} - u'\ _2}{\ u'\ _2}$	$\frac{\ au'_{H/2} - au'\ _2}{\ au'\ _2}$	$\ u_{H/2} - u\ _\infty$	$\ u'_{H/2} - u'\ _\infty$	$\ au'_{H/2} - au'\ _\infty$	κ	$\frac{a_{\max}}{a_{\min}}$
1/2	1.0E+00	1.0E+00	1.0E+00	3.2E+02	3.3E+03	3.3E-01	5.8E+00	1.0E+08
1/2 ²	1.0E+00	1.0E+00	1.0E+00	3.2E+02	3.3E+03	3.3E-01	2.5E+01	1.0E+08
1/2 ³	1.0E+00	1.0E+00	1.0E+00	3.2E+02	3.3E+03	3.3E-01	1.0E+02	1.0E+08
1/2 ⁴	1.0E+00	1.0E+00	1.0E+00	3.2E+02	3.3E+03	3.3E-01	4.1E+02	1.0E+08
1/2 ⁵	1.0E+00	1.0E+00	1.0E+00	3.2E+02	3.3E+03	3.3E-01	1.7E+03	1.0E+08
1/2 ⁶	1.0E+00	1.0E+00	1.0E+00	3.2E+02	3.3E+03	3.3E-01	6.6E+03	1.0E+08

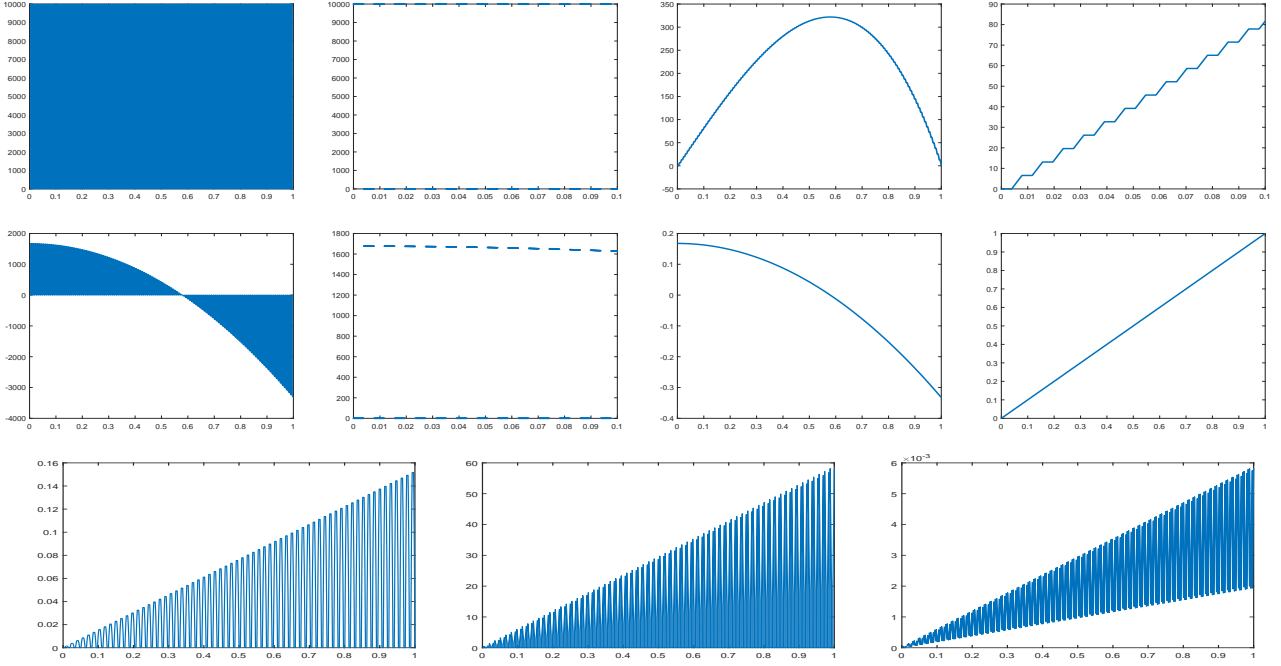


FIGURE 7. Example 2: The top row: a in $[0,1]$ (first panel), a in $[0,0.1]$ (second panel), u in $[0,1]$ (third panel), and u in $[0,0.1]$ (fourth panel). The middle row: u' in $[0,1]$ (first panel), u' in $[0,0.1]$ (second panel), au' in $[0,1]$ (third panel), and f in $[0,1]$ (fourth panel). The bottom row: $|\tilde{u}_H - u|$ (first panel), $|\tilde{u}'_H - u'|$ (second panel), and $|a\tilde{u}'_H - au'|$ (third panel) in $[0,1]$ with $H = \frac{1}{2^6}$ at all $x_i = i/N$ for $i = 0, \dots, N$ with $N = 2^{14}$ in (3.1).

Example 3. Consider $f(x) = 1$ and a continuous diffusion coefficient $a(x) = \frac{1}{x^2} \frac{1}{1.05 + \sin(2^{10}\pi x)}$ with the high-frequency oscillation. Note that $\lim_{x \rightarrow 0^+} a(x) = \infty$. Then the exact solution u of (1.1) can be expressed as

$$\begin{aligned}
 u(x) = & \frac{-c_1 r_1 x^3}{3} - \frac{r_1 x^4}{4} + \frac{c_1 x^2 \cos(r_2 x)}{r_2} - \frac{2c_1 \cos(r_2 x)}{r_2^3} - \frac{2c_1 x \sin(r_2 x)}{r_2^2} \\
 & + \frac{x^3 \cos(r_2 x)}{r_2} - \frac{3x^2 \sin(r_2 x)}{r_2^2} + \frac{6 \sin(r_2 x)}{r_2^4} - \frac{6x \cos(r_2 x)}{r_2^3} + c_2,
 \end{aligned} \tag{3.5}$$

where $r_1 = 1.05$, $r_2 = 2^{10}\pi$, and the constants c_1, c_2 can be uniquely determined by imposing the boundary condition $u(0) = u(1) = 0$. The results on numerical solutions \tilde{u}_H and $u_{H/2}$ are presented in Tables 7 to 9 and Fig. 8.

3.2. The exact solution u is not available.

Example 4. Consider $f(x) = \sin(2x) \cos(x)$ and a continuous coefficient

$$a(x) = 2 \exp(1) + \sin(2^9 \pi x) \exp(x^2) \cos(10x),$$

with the high-frequency oscillation. Note that the exact solution u of (1.1) is not available. The results on the numerical solution \tilde{u}_H are presented in Tables 10 and 11 and Fig. 9.

Example 5. Consider $f(x) = \cos(4x)$ and a discontinuous diffusion coefficient a with high-contrast jumps below:

$$a(x) = \left(10^4 \chi_{[\frac{i-1}{2^8}, \frac{i}{2^8})} + 10^{-4} \chi_{[\frac{i}{2^8}, \frac{i+1}{2^8})} \right) \exp(x^2 + 1) (10 + \cos(20x)) \quad \text{with } i = 1, 3, 5, \dots, 2^8 - 1.$$

Note that the exact solution u of (1.1) is not available. The results on the numerical solution \tilde{u}_H are presented in Tables 12 and 13 and Fig. 10.

TABLE 7. Performance of the l_2 norm of the error in Example 3 of our proposed derivative-orthogonal wavelet multiscale method on the uniform Cartesian mesh H . Note that $N = 2^{15}$ in (3.1) for estimating the l_2 norm. Since $\lim_{x \rightarrow 0^+} a(x) = \infty$, we replace $\sum_{i=0}^N$ by $\sum_{i=1}^N$ in $\frac{\|\tilde{u}'_H - au'\|_2}{\|au'\|_2}$ in (3.2), and $a_{\max} = \max_{2^{-15} \leq x \leq 1} a(x)$.

H	$\frac{\ \tilde{u}_H - u\ _2}{\ u\ _2}$	order	$\frac{\ \tilde{u}'_H - u'\ _2}{\ u'\ _2}$	order	$\frac{\ \tilde{a}\tilde{u}'_H - au'\ _2}{\ au'\ _2}$	order	κ	$\frac{a_{\max}}{a_{\min}}$
1/2	4.7851E-01		7.3506E-01		4.0353E+00		1.2E+05	1.9E+09
1/2 ²	1.3535E-01	1.82	4.2175E-01	0.80	5.3416E-01	2.92	7.2E+05	1.9E+09
1/2 ³	3.5206E-02	1.94	2.1820E-01	0.95	1.0874E-01	2.30	2.2E+06	1.9E+09
1/2 ⁴	8.9328E-03	1.98	1.1000E-01	0.99	4.7332E-02	1.20	5.2E+06	1.9E+09
1/2 ⁵	2.2461E-03	1.99	5.5063E-02	1.00	2.3678E-02	1.00	1.1E+07	1.9E+09
1/2 ⁶	5.6249E-04	2.00	2.7445E-02	1.00	1.1889E-02	0.99	2.4E+07	1.9E+09
1/2 ⁷	1.4022E-04	2.00	1.3521E-02	1.02	5.9820E-03	0.99	4.9E+07	1.9E+09

TABLE 8. Performance of the l_∞ norm of the error in Example 3 of our proposed derivative-orthogonal wavelet multiscale method on the uniform Cartesian mesh H . Note that $N = 2^{15}$ in (3.1) for estimating the l_∞ norm. Since $\lim_{x \rightarrow 0^+} a(x) = \infty$, we replace $\max_{0 \leq i \leq N}$ by $\max_{1 \leq i \leq N}$ in $\|\tilde{a}\tilde{u}'_H - au'\|_\infty$ in (3.3), and $a_{\max} = \max_{2^{-15} \leq x \leq 1} a(x)$.

H	$\ \tilde{u}_H - u\ _\infty$	order	$\ \tilde{u}'_H - u'\ _\infty$	order	$\ \tilde{a}\tilde{u}'_H - au'\ _\infty$	order	κ	$\frac{a_{\max}}{a_{\min}}$
1/2	1.5972E-02		3.6152E-01		2.6852E+02		1.2E+05	1.9E+09
1/2 ²	5.8117E-03	1.46	2.1609E-01	0.74	3.3392E+01	3.01	7.2E+05	1.9E+09
1/2 ³	1.7303E-03	1.75	1.1623E-01	0.89	3.6502E+00	3.19	2.2E+06	1.9E+09
1/2 ⁴	4.7107E-04	1.88	5.9318E-02	0.97	2.5125E-01	3.86	5.2E+06	1.9E+09
1/2 ⁵	1.2284E-04	1.94	2.9109E-02	1.03	6.4687E-02	1.96	1.1E+07	1.9E+09
1/2 ⁶	3.1387E-05	1.97	1.4016E-02	1.05	5.4947E-02	0.24	2.4E+07	1.9E+09
1/2 ⁷	7.9477E-06	1.98	6.2779E-03	1.16	2.9363E-02	0.90	4.9E+07	1.9E+09

TABLE 9. Performance of l_2 and l_∞ norms of the error in Example 3 of the standard second-order FEM on the uniform Cartesian mesh H . Note that $N = 2^{15}$ in (3.1) for estimating l_2 and l_∞ norms. Since $\lim_{x \rightarrow 0^+} a(x) = \infty$, we replace $\sum_{i=0}^N$ by $\sum_{i=1}^N$ and $\max_{0 \leq i \leq N}$ by $\max_{1 \leq i \leq N}$ in the following $\frac{\|au'_{H/2} - au'\|_2}{\|au'\|_2}$ and $\|au'_{H/2} - au'\|_\infty$ errors, and $a_{\max} = \max_{2^{-15} \leq x \leq 1} a(x)$.

H	$\frac{\ u_{H/2} - u\ _2}{\ u\ _2}$	$\frac{\ u'_{H/2} - u'\ _2}{\ u'\ _2}$	$\frac{\ au'_{H/2} - au'\ _2}{\ au'\ _2}$	$\ u_{H/2} - u\ _\infty$	$\ u'_{H/2} - u'\ _\infty$	$\ au'_{H/2} - au'\ _\infty$	κ	$\frac{a_{\max}}{a_{\min}}$
1/2	7.8E-01	8.7E-01	1.5E+01	2.1E+01	4.8E+02	1.0E+06	6.1E+04	1.9E+09
1/2 ²	7.1E-01	8.2E-01	8.3E+00	2.0E+01	4.6E+02	5.5E+05	4.9E+05	1.9E+09
1/2 ³	7.0E-01	8.1E-01	4.5E+00	1.9E+01	4.4E+02	2.9E+05	3.9E+06	1.9E+09
1/2 ⁴	7.0E-01	8.0E-01	2.6E+00	1.9E+01	4.4E+02	1.5E+05	3.1E+07	1.9E+09
1/2 ⁵	6.9E-01	8.0E-01	1.9E+00	1.9E+01	4.3E+02	7.4E+04	2.5E+08	1.9E+09
1/2 ⁶	6.9E-01	8.0E-01	1.6E+00	1.9E+01	4.3E+02	3.7E+04	2.0E+09	1.9E+09
1/2 ⁷	6.9E-01	8.0E-01	1.5E+00	1.9E+01	4.3E+02	1.8E+04	1.6E+10	1.9E+09

Example 6. Consider a discontinuous source term $f(x)$ and a discontinuous diffusion coefficient $a(x)$ with high-contrast jumps below:

$$a(x) = \left(10^4 \chi_{[\frac{i-1}{2^8}, \frac{i}{2^8})} + 10^{-4} \chi_{[\frac{i}{2^8}, \frac{i+1}{2^8})} \right) (10 + \sin(40x)) \quad \text{with } i = 1, 3, 5, \dots, 2^8 - 1,$$

$$f(x) = \left(1 \chi_{[\frac{i-1}{2^8}, \frac{i}{2^8})} + 10^{-3} \chi_{[\frac{i}{2^8}, \frac{i+1}{2^8})} \right) \cos(10x) \quad \text{with } i = 1, 3, 5, \dots, 2^8 - 1.$$

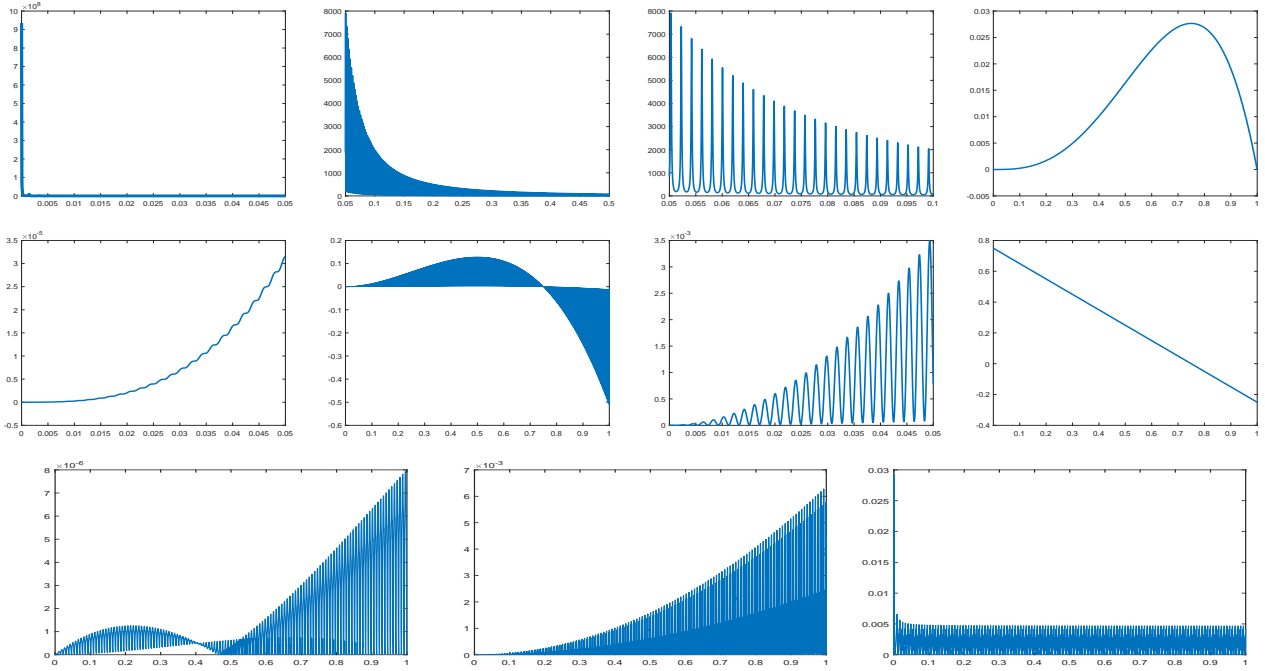


FIGURE 8. Example 3: The top row: a in $[2^{-15}, 0.05]$ (first panel), a in $[0.05, 0.1]$ (second panel), a in $[0.05, 0.1]$ (third panel), and u in $[0, 1]$ (fourth panel). The middle row: u in $[0, 0.05]$ (first panel), u' in $[0, 1]$ (second panel), u' in $[0, 0.05]$ (third panel), and au' in $[2^{-15}, 1]$ (fourth panel). The bottom row: $|\tilde{u}_H - u|$ (first panel) in $[0, 1]$, $|\tilde{u}'_H - u'|$ (second panel) in $[0, 1]$, and $|a\tilde{u}'_H - au'|$ (third panel) in $[2^{-15}, 1]$ with $H = \frac{1}{2^7}$ at all $x_i = i/N$, $i = 0, 1, \dots, N$ with $N = 2^{15}$ in (3.1).

TABLE 10. Performance of the l_2 norm of the error in Example 4 of our proposed derivative-orthogonal wavelet multiscale method on the uniform Cartesian mesh H . Note that $N = 2^{14}$ in (3.1) for estimating the l_2 norm.

H	$\frac{\ \tilde{u}_H - \tilde{u}_{H/2}\ _2}{\ \tilde{u}_{H/2}\ _2}$	order	$\frac{\ \tilde{u}'_H - \tilde{u}'_{H/2}\ _2}{\ \tilde{u}'_{H/2}\ _2}$	order	$\frac{\ a\tilde{u}'_H - a\tilde{u}'_{H/2}\ _2}{\ a\tilde{u}'_{H/2}\ _2}$	order	κ	$\frac{a_{\max}}{a_{\min}}$
1/2	2.3154E-01		4.5360E-01		4.5866E-01		1.54	2.67
1/2 ²	4.7958E-02	2.27	2.0709E-01	1.13	2.1327E-01	1.10	1.81	2.67
1/2 ³	1.1535E-02	2.06	1.0093E-01	1.04	1.0325E-01	1.05	1.93	2.67
1/2 ⁴	3.1247E-03	1.88	5.0224E-02	1.01	5.1273E-02	1.01	1.97	2.67
1/2 ⁵	8.2435E-04	1.92	2.5085E-02	1.00	2.5615E-02	1.00	1.99	2.67
1/2 ⁶	2.1331E-04	1.95	1.2539E-02	1.00	1.2807E-02	1.00	1.99	2.67

TABLE 11. Performance of the l_∞ norm of the error in Example 4 of our proposed derivative-orthogonal wavelet multiscale method on the uniform Cartesian mesh H . Note that $N = 2^{14}$ in (3.1) for estimating the l_∞ norm.

H	$\ \tilde{u}_H - \tilde{u}_{H/2}\ _\infty$	order	$\ \tilde{u}'_H - \tilde{u}'_{H/2}\ _\infty$	order	$\ a\tilde{u}'_H - a\tilde{u}'_{H/2}\ _\infty$	order	κ	$\frac{a_{\max}}{a_{\min}}$
1/2	4.2314E-03		2.5856E-02		1.0052E-01		1.54	2.67
1/2 ²	1.0619E-03	1.99	1.5628E-02	0.73	6.3632E-02	0.66	1.81	2.67
1/2 ³	2.7613E-04	1.94	6.6146E-03	1.24	2.6730E-02	1.25	1.93	2.67
1/2 ⁴	8.7980E-05	1.65	3.0974E-03	1.09	1.2096E-02	1.14	1.97	2.67
1/2 ⁵	2.4401E-05	1.85	1.5457E-03	1.00	6.5000E-03	0.90	1.99	2.67
1/2 ⁶	6.4601E-06	1.92	7.7127E-04	1.00	3.6661E-03	0.83	1.99	2.67

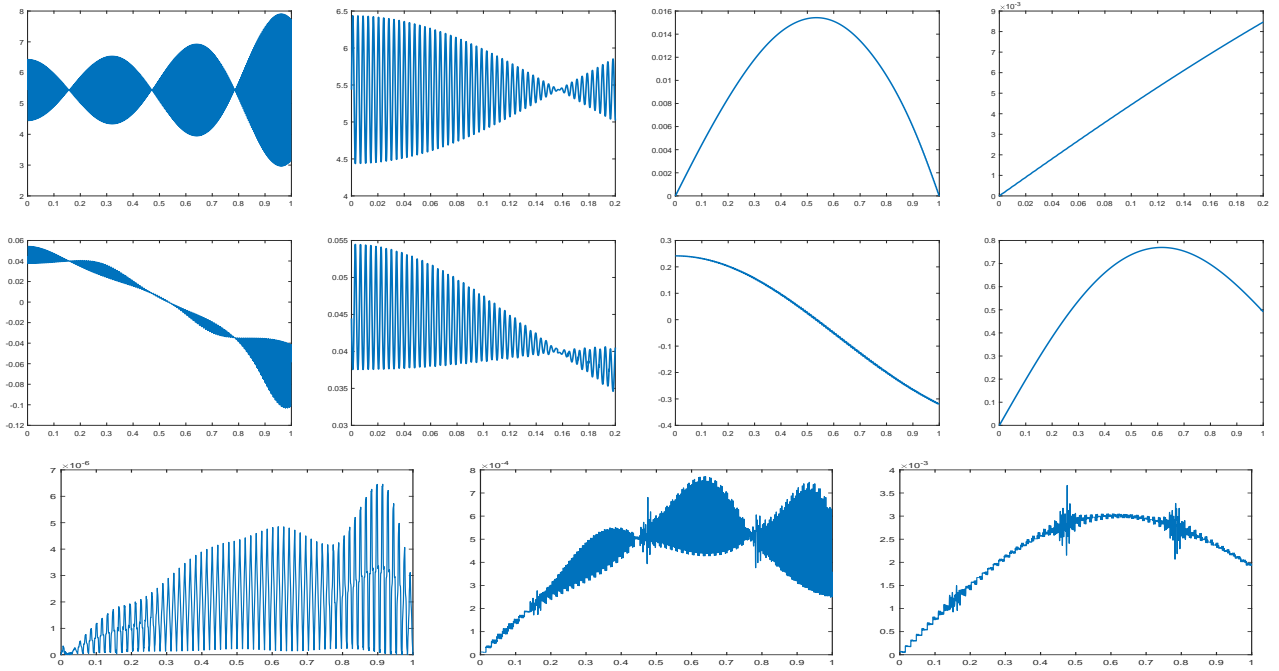


FIGURE 9. Example 4: The top row: a in $[0,1]$ (first panel), a in $[0,0.2]$ (second panel), \tilde{u}_H in $[0,1]$ (third panel), and \tilde{u}_H in $[0,0.2]$ (fourth panel). The middle row: \tilde{u}'_H in $[0,1]$ (first panel), \tilde{u}'_H in $[0,0.2]$ (second panel), $a\tilde{u}'_H$ in $[0,1]$ (third panel) with $H = \frac{1}{2^7}$, and f in $[0,1]$ (fourth panel). The bottom row: $|\tilde{u}_H - \tilde{u}_{H/2}|$ (first panel), $|\tilde{u}'_H - \tilde{u}'_{H/2}|$ (second panel), and $|a\tilde{u}'_H - a\tilde{u}'_{H/2}|$ (third panel) in $[0,1]$ with $H = \frac{1}{2^6}$ at all $x_i = i/N$ for $i = 0, \dots, N$ with $N = 2^{14}$ in (3.1).

TABLE 12. Performance of the l_2 norm of the error in Example 5 of our proposed derivative-orthogonal wavelet multiscale method on the uniform Cartesian mesh H . Note that $N = 2^{14}$ in (3.1) for estimating the l_2 norm.

H	$\frac{\ \tilde{u}_H - \tilde{u}_{H/2}\ _2}{\ \tilde{u}_{H/2}\ _2}$	order	$\frac{\ \tilde{u}'_H - \tilde{u}'_{H/2}\ _2}{\ \tilde{u}'_{H/2}\ _2}$	order	$\frac{\ a\tilde{u}'_H - a\tilde{u}'_{H/2}\ _2}{\ a\tilde{u}'_{H/2}\ _2}$	order	κ	$\frac{a_{\max}}{a_{\min}}$
$1/2$	8.1846E-01		1.6153E+00		1.1281E+00		1.1951E+08	3.0665E+08
$1/2^2$	1.7618E-01	2.22	4.9703E-01	1.70	3.8735E-01	1.54	1.2820E+08	3.0665E+08
$1/2^3$	3.8195E-02	2.21	2.3071E-01	1.11	1.8159E-01	1.09	1.3075E+08	3.0665E+08
$1/2^4$	8.6474E-03	2.14	1.1397E-01	1.02	8.9408E-02	1.02	1.3136E+08	3.0665E+08
$1/2^5$	2.1766E-03	1.99	5.6825E-02	1.00	4.4544E-02	1.01	1.3151E+08	3.0665E+08
$1/2^6$	5.9792E-04	1.86	2.8394E-02	1.00	2.2252E-02	1.00	1.3155E+08	3.0665E+08

TABLE 13. Performance of the l_∞ norm of the error in Example 5 of our proposed derivative-orthogonal wavelet multiscale method on the uniform Cartesian mesh H . Note that $N = 2^{14}$ in (3.1) for estimating the l_∞ norm.

H	$\ \tilde{u}_H - \tilde{u}_{H/2}\ _\infty$	order	$\ \tilde{u}'_H - \tilde{u}'_{H/2}\ _\infty$	order	$\ a\tilde{u}'_H - a\tilde{u}'_{H/2}\ _\infty$	order	κ	$\frac{a_{\max}}{a_{\min}}$
$1/2$	3.0071E+00		2.9791E+01		1.3141E-01		1.1951E+08	3.0665E+08
$1/2^2$	9.5963E-01	1.65	2.4180E+01	0.30	7.0859E-02	0.89	1.2820E+08	3.0665E+08
$1/2^3$	2.4780E-01	1.95	1.2500E+01	0.95	3.3683E-02	1.07	1.3075E+08	3.0665E+08
$1/2^4$	6.9096E-02	1.84	5.7479E+00	1.12	1.6012E-02	1.07	1.3136E+08	3.0665E+08
$1/2^5$	1.8739E-02	1.88	2.7866E+00	1.04	7.8678E-03	1.03	1.3151E+08	3.0665E+08
$1/2^6$	4.8165E-03	1.96	1.3783E+00	1.02	3.9355E-03	1.00	1.3155E+08	3.0665E+08

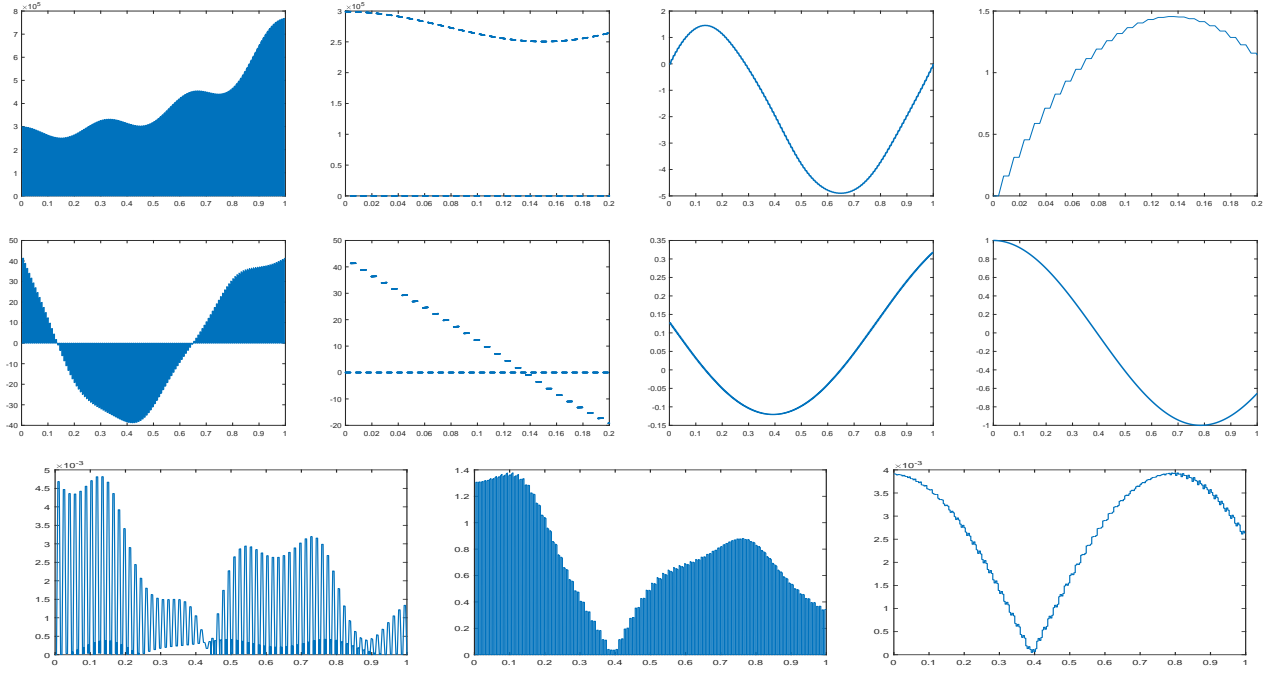


FIGURE 10. Example 5: The top row: a in $[0,1]$ (first panel), a in $[0,0.2]$ (second panel), \tilde{u}_H in $[0,1]$ (third panel), and \tilde{u}_H in $[0,0.2]$ (fourth panel). The middle row: \tilde{u}'_H in $[0,1]$ (first panel), \tilde{u}'_H in $[0,0.2]$ (second panel), $a\tilde{u}'_H$ in $[0,1]$ (third panel) with $H = \frac{1}{2^7}$, and f in $[0,1]$ (fourth panel). The bottom row: $|\tilde{u}_H - \tilde{u}_{H/2}|$ (first panel), $|\tilde{u}'_H - \tilde{u}'_{H/2}|$ (second panel), and $|a\tilde{u}'_H - a\tilde{u}'_{H/2}|$ (third panel) in $[0,1]$ with $H = \frac{1}{2^6}$ at all $x_i = i/N$ for $i = 0, \dots, N$ with $N = 2^{14}$ in (3.1).

Note that the exact solution u of (1.1) is not available and $\|f\|_{L_2(\Omega)} \approx 0.511567$. The results on the numerical solution \tilde{u}_H are presented in Tables 14 and 15 and Fig. 11.

TABLE 14. Performance of the l_2 norm of the error in Example 6 of our proposed derivative-orthogonal wavelet multiscale method on the uniform Cartesian mesh H . Note that $N = 2^{14}$ in (3.1) for estimating the l_2 norm.

H	$\frac{\ \tilde{u}_H - \tilde{u}_{H/2}\ _2}{\ \tilde{u}_{H/2}\ _2}$	order	$\frac{\ \tilde{u}'_H - \tilde{u}'_{H/2}\ _2}{\ \tilde{u}'_{H/2}\ _2}$	order	$\frac{\ a\tilde{u}'_H - a\tilde{u}'_{H/2}\ _2}{\ a\tilde{u}'_{H/2}\ _2}$	order	κ	$\frac{a_{\max}}{a_{\min}}$
$1/2$	5.1083E+00		1.0242E+01		1.0776E+01		1.0159E+08	1.2222E+08
$1/2^2$	4.9138E-01	3.38	9.4325E-01	3.44	9.4667E-01	3.51	1.0232E+08	1.2222E+08
$1/2^3$	1.0610E-01	2.21	3.5600E-01	1.41	3.5931E-01	1.40	1.0788E+08	1.2222E+08
$1/2^4$	2.7615E-02	1.94	1.7106E-01	1.06	1.7199E-01	1.06	1.0933E+08	1.2222E+08
$1/2^5$	6.6613E-03	2.05	8.4581E-02	1.02	8.5132E-02	1.01	1.0955E+08	1.2222E+08
$1/2^6$	1.8051E-03	1.88	4.2198E-02	1.00	4.2466E-02	1.00	1.0963E+08	1.2222E+08

4. CONCLUSION

In this paper, we consider $-\nabla \cdot (a\nabla u) = f$ with the zero Dirichlet boundary condition, $0 < a_{\min} \leq a \leq a_{\max} < \infty$, and $f \in L_2(\Omega)$ in the one-dimensional domain $\Omega = (0, 1)$. To numerically compute a precise and convincing approximated solution on the coarse mesh size H , we present an innovative derivative-orthogonal wavelet multiscale method to calculate the numerical solution \tilde{u}_H . The main contributions of our proposed method are as follows:

Contributions in the theoretical analysis:

TABLE 15. Performance of the l_∞ norm of the error in Example 6 of our proposed derivative-orthogonal wavelet multiscale method on the uniform Cartesian mesh H . Note that $N = 2^{14}$ in (3.1) for estimating the l_∞ norm.

H	$\ \tilde{u}_H - \tilde{u}_{H/2}\ _\infty$	order	$\ \tilde{u}'_H - \tilde{u}'_{H/2}\ _\infty$	order	$\ a\tilde{u}'_H - a\tilde{u}'_{H/2}\ _\infty$	order	κ	$\frac{a_{\max}}{a_{\min}}$
1/2	3.6544E+00		3.2872E+01		2.9586E-02		1.0159E+08	1.2222E+08
1/2 ²	1.7343E+00	1.08	3.1000E+01	0.08	2.8427E-02	0.06	1.0232E+08	1.2222E+08
1/2 ³	4.8819E-01	1.83	1.6754E+01	0.89	1.6690E-02	0.77	1.0788E+08	1.2222E+08
1/2 ⁴	1.2856E-01	1.92	8.3965E+00	1.00	7.8405E-03	1.09	1.0933E+08	1.2222E+08
1/2 ⁵	3.6352E-02	1.82	4.2650E+00	0.98	3.9594E-03	0.99	1.0955E+08	1.2222E+08
1/2 ⁶	9.4345E-03	1.95	2.1079E+00	1.02	1.9999E-03	0.99	1.0963E+08	1.2222E+08

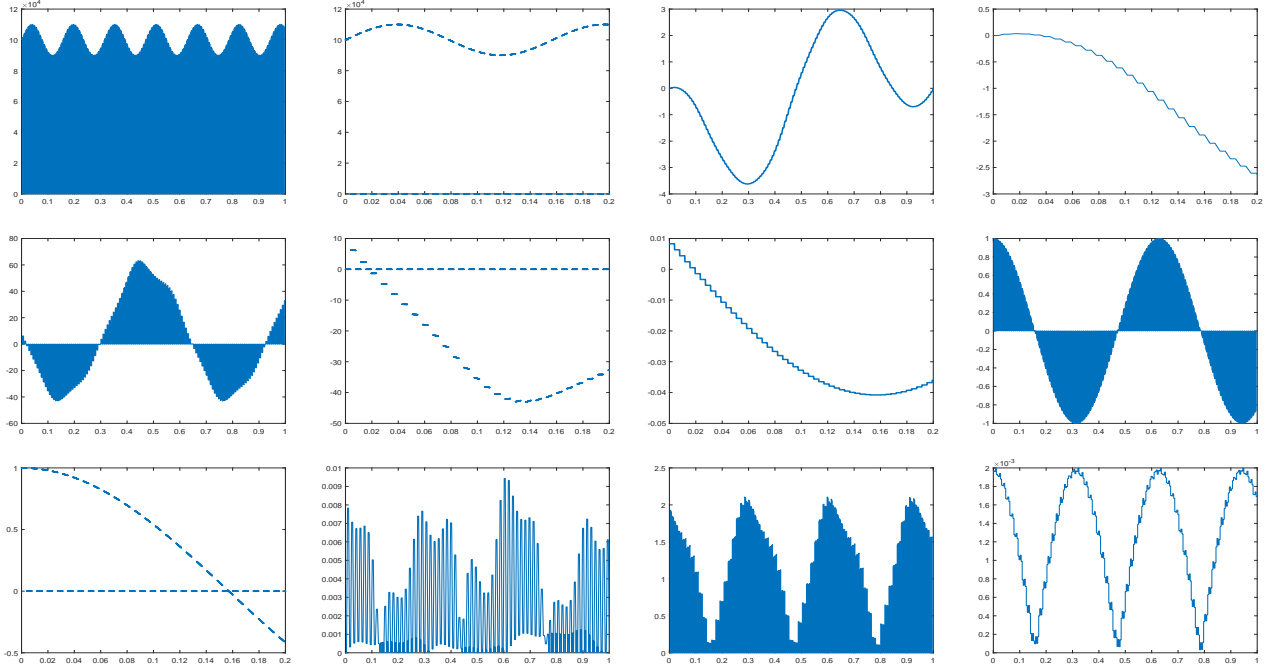


FIGURE 11. Example 6: The top row: a in $[0,1]$ (first panel), a in $[0,0.2]$ (second panel), \tilde{u}_H in $[0,1]$ (third panel), and \tilde{u}_H in $[0,0.2]$ (fourth panel). The middle row: \tilde{u}'_H in $[0,1]$ (first panel), \tilde{u}'_H in $[0,0.2]$ (second panel), $a\tilde{u}'_H$ in $[0,0.2]$ (third panel) with $H = \frac{1}{2^7}$, and f in $[0,1]$ (fourth panel). The bottom row: f in $[0,0.2]$ (first panel), $|\tilde{u}_H - \tilde{u}_{H/2}|$ (second panel), $|\tilde{u}'_H - \tilde{u}'_{H/2}|$ (third panel), and $|a\tilde{u}'_H - a\tilde{u}'_{H/2}|$ (fourth panel) in $[0,1]$ with $H = \frac{1}{2^6}$ at all $x_i = i/N$ for $i = 0, \dots, N$ with $N = 2^{14}$ in (3.1).

- We prove in Theorem 2.2 that the condition number κ of the stiffness matrix of our proposed method satisfies that $\kappa \leq \frac{a_{\max}}{a_{\min}}$ for any coarse mesh size H .
- We establish in Theorem 2.5 that the energy norm of the error of our proposed method attains the first-order convergence rate for any coarse mesh size H . Precisely, we prove that $\|\sqrt{a}(u' - (\tilde{u}_H)')\|_{L_2(\Omega)} \leq CH$, where $C = \frac{2}{\sqrt{a_{\min}}}\|f\|_{L_2(\Omega)}$.
- We prove in Theorem 2.6 that the L_2 norm of the error of our proposed method achieves the second-order convergence rate for any coarse mesh size H . Precisely, we prove that $\|u - \tilde{u}_H\|_{L_2(\Omega)} \leq CH^2$, where $C = \frac{4}{a_{\min}}\|f\|_{L_2(\Omega)}$.
- The explicit expressions of constants C in error estimates indicate that the energy and L_2 -norm errors of our proposed method are independent to a_{\max} . Hence, our method can handle simultaneously the rough diffusion coefficient a and the rough source term f , as long as $\|f\|_{L_2(\Omega)}$ is not huge.

- We prove in Theorem 2.8 that our numerical solutions \tilde{u}_H have the interpolation property in (2.64).

Contributions in the numerical computation:

- We provide several examples (u is available/unavailable, a is continuous/discontinuous, and $\lim_{x \rightarrow 0^+} a(x) = \infty$) to measure $\frac{\|\tilde{u}_H - u\|_2}{\|u\|_2}$, $\frac{\|\tilde{u}'_H - u'\|_2}{\|u'\|_2}$, $\frac{\|a\tilde{u}'_H - au'\|_2}{\|au'\|_2}$, $\|\tilde{u}_H - u\|_\infty$, $\|\tilde{u}'_H - u'\|_\infty$, and $\|a\tilde{u}'_H - au'\|_\infty$. The numerical results confirm bounded condition numbers and first-order/second-order convergence rates of the proposed method for elliptic equations with high-frequency and high-contrast coefficients.
- Particularly, the coefficient a satisfies that $a_{\max} = \sup_{x \in \Omega} a(x) = \infty$ in Example 3, and the coefficient a and the source term f both exhibit discontinuous and high-frequency oscillations and high-contrast jumps with $\|f\|_{L_2(\Omega)} \approx 0.5$ in Example 6. Our proposed method continues to perform robustly.
- Our derivative-orthogonal wavelet multiscale method is straightforward to be implemented, allowing for easy repetition and verification of the numerical results.

In the future, we plan to extend our proposed derivative-orthogonal wavelet multiscale method presented in this paper to the 2D case of (1.1) by modifying the regular and special basis functions.

Acknowledgment

Michael Neilan (neilan@pitt.edu, Department of Mathematics, University of Pittsburgh, Pittsburgh, PA 15260 USA) provided the initial idea and proof of Theorem 2.8 (the interpolation property) and recommended testing Example 3 with $\lim_{x \rightarrow 0^+} a(x) = \infty$ to verify the robustness of the proposed derivative-orthogonal wavelet multiscale method.

REFERENCES

- [1] A. Ali, H. Mankad, F. Pereira, and F. S. Sousa, The multiscale perturbation method for second order elliptic equations. *Appl. Math. Comput.* **387** (2020), 125023.
- [2] G. Allaire, and R. Brizzi, A multiscale finite element method for numerical homogenization. *SIAM Multiscale Model. Simul.* **4** (2005), 790-812.
- [3] T. Arbogast, Z. Tao, and H. Xiao, Multiscale mortar mixed methods for heterogeneous elliptic problems. *Contemp. Math.* **586** (2013), 9-21.
- [4] T. Arbogast and H. Xiao, A Multiscale Mortar Mixed Space Based on Homogenization for Heterogeneous Elliptic Problems. *SIAM J. Numer. Anal.* **51** (2013), 377-399.
- [5] T. Arbogast and H. Xiao, Two-level mortar domain decomposition preconditioners for heterogeneous elliptic problems. *Comput. Methods Appl. Mech. Engrg.* **292** (2015), 221-242.
- [6] M. Blumenfeld, The regularity of interface-problems on corner-regions. *Lecture Notes in Math.* **1121** (1985), 38-54.
- [7] R. Butler, T. Dodwell, A. Reinarz, A. Sandhu, R. Scheichl, and L. Seelinger, High-performance dune modules for solving large-scale, strongly anisotropic elliptic problems with applications to aerospace composites. *Comput. Phys. Commun.* **249** (2020), 106997.
- [8] Z. Cai and S. Kim, A finite element method using singular functions for the Poisson equation: corner singularities. *SIAM J. Numer. Anal.* **39** (2001), no. 1, 286-299.
- [9] C. C. Chu, I. G. Graham, and T. Y. Hou, A new multiscale finite element method for high-contrast elliptic interface problems. *Math. Comput.* **79** (2010), 1915-1955.
- [10] C. Engwer, P. Henning, A. Målqvist, and D. Peterseim, Efficient implementation of the localized orthogonal decomposition method. *Comput. Methods Appl. Mech. Engrg.* **350** (2019), 123-153.
- [11] G. J. Fix, S. Gulati and G. I. Wakoff, On the use of singular functions with finite element approximations. *J. Comput. Phys.* **13** (1973), 209-228.
- [12] S. Fu, E. Chung, and G. Li, Edge multiscale methods for elliptic problems with heterogeneous coefficients. *J. Comput. Phys.* **396** (2019), 228-242.
- [13] R. T. Guiraldello, R. F. Ausas, F. S. Sousa, F. Pereira, and G. C. Buscaglia, Interface spaces for the Multiscale Robin Coupled Method in reservoir simulation. *Math. Comput. Simul.* **164** (2019), 103-119.
- [14] B. Han, *Framelets and wavelets: algorithms, analysis, and applications*. Applied and Numerical Harmonic Analysis. Birkhäuser/Springer, Cham, 2017. xxxiii + 724 pp.
- [15] B. Han and M. Michelle, Derivative-orthogonal Riesz wavelets in Sobolev spaces with applications to differential equations. *Appl. Comput. Harmon. Anal.* **47** (2019), 759-794.

- [16] F. Hellman and A. Målqvist, Contrast independent localization of multiscale problems. *SIAM Multiscale Model. Simul.* **15** (2017), 1325-1355.
- [17] T. Y. Hou and X. H. Wu, A multiscale finite element method for elliptic problems in composite materials and porous media. *J. Comput. Phys.* **134** (1997), 169-189.
- [18] T. Y. Hou, X. H. Wu, and Z. Cai, Convergence of a multiscale finite element method for elliptic problems with rapidly oscillating coefficients. *Math. Comput.* **68** (1999), 913-943.
- [19] T. Y. Hou, F. N. Hwang, P. Liu, and C. C. Yao, An iteratively adaptive multi-scale finite element method for elliptic PDEs with rough coefficients. *J. Comput. Phys.* **336** (2017), 375-400.
- [20] A. Jaramillo, R. T. Guiraldello, S. Paz, R. F. Ausas, F. S. Sousa, F. Pereira, and G. C. Buscaglia, Towards HPC simulations of billion-cell reservoirs by multiscale mixed methods. *Comput. Geosci.* **26** (2022), 481-501.
- [21] P. Jenny, S. H. Lee, and H. A. Tchelepi, Adaptive multiscale finite-volume method for multiphase flow and transport in porous media. *SIAM Multiscale Model. Simul.* **3** (2004), 50-64.
- [22] R. B. Kellogg, Singularities in interface problems. *Numerical Solution of Partial Differential Equations-II* (1971), 351-400.
- [23] R. B. Kellogg, Higher order singularities for interface problems. *The Mathematical Foundations of the Finite Element Method with Applications to Partial Differential Equations* (1972), 589-602.
- [24] R. B. Kellogg, On the Poisson equation with intersecting interfaces. *Appl. Anal.* **4** (1975), no. 2, 101-129.
- [25] S. Kim, Z. Cai, J. Pyo and S. Kong, A finite element method using singular functions: interface problems. *Hokkaido Math. J.* **36** (2007), no. 4, 815-836.
- [26] S. Kim and S. Kong, A finite element method dealing the singular points with a cut-off function. *J. Appl. Math. Comput.* **21** (2006), no. 1-2, 141-152.
- [27] V. Kippe, J. E. Aarnes, and K. A. Lie, A comparison of multiscale methods for elliptic problems in porous media flow. *Comput. Geosci.* **12** (2008), 377-398.
- [28] G. Li and J. Hu, Wavelet-based edge multiscale parareal algorithm for parabolic equations with heterogeneous coefficients and rough initial data. *J. Comput. Phys.* **444** (2021), 110572.
- [29] A. Målqvist and A. Persson, Multiscale techniques for parabolic equations. *Numer. Math.* **138** (2018), 191-217.
- [30] A. Målqvist and D. Peterseim, Localization of elliptic multiscale problems. *Math. Comput.* **83** (2014), 2583-2603.
- [31] P. Mineev, S. Srinivasan, and P. N. Vabishchevich, Flux formulation of parabolic equations with highly heterogeneous coefficients. *J. Comput. Appl. Math.* **340** (2018), 582-601.
- [32] S. Nicaise, Polygonal interface problems: higher regularity results. *Commun. Partial. Differ. Equ.* **15** (1990), no. 10, 1475-1508.
- [33] S. Nicaise and A. M. Sandig, General interface problems-I. *Math. Methods Appl. Sci.* **17** (1994), 395-429.
- [34] J. Nolen, G. Papanicolaou, and O. Pironneau, A framework for adaptive multiscale methods for elliptic problems. *SIAM Multiscale Model. Simul.* **7** (2008), 171-196.
- [35] M. Petzoldt, Regularity results for Laplace interface problems in two dimensions. *J. Anal. Appl.* **20** (2001), no. 2, 431-455.
- [36] M. Petzoldt, A posteriori error estimators for elliptic equations with discontinuous coefficients. *Adv. Comput. Math.* **16** (2002), no. 1, 47-75.
- [37] D. A. Di Pietro and A. Ern, Mathematical aspects of discontinuous Galerkin methods. *Springer Berlin, Heidelberg*. 2012.
- [38] M. R. Rasaei and M. Sahimi, Upscaling and simulation of waterflooding in heterogeneous reservoirs using wavelet transformations: application to the SPE-10 model. *Transp. Porous. Med.* **72** (2008), 311-338.
- [39] S. Srinivasan, R. Lazarov, and P. Mineev, Multiscale direction-splitting algorithms for parabolic equations with highly heterogeneous coefficients. *Comput. Math. Appl.* **72** (2016), 1641-1654.
- [40] P. Tahmasebi and S. Kamrava, A multiscale approach for geologically and flow consistent modeling. *Transp. Porous. Med.* **124** (2018), 237-261.
- [41] J. L. Vázquez, The Porous medium equation: mathematical theory. *Clarendon Press*. 2007.
- [42] Z. Zhang, M. Ci, and T. Y. Hou, A multiscale data-driven stochastic method for elliptic PDEs with random coefficients. *SIAM Multiscale Model. Simul.* **13** (2015), 173-204.

DEPARTMENT OF MATHEMATICS, UNIVERSITY OF PITTSBURGH, PITTSBURGH, PA 15260 USA. qif21@pitt.edu, fengq2023@gmail.com

DEPARTMENT OF MATHEMATICAL AND STATISTICAL SCIENCES, UNIVERSITY OF ALBERTA, EDMONTON, ALBERTA, CANADA T6G 2G1. bhan@ualberta.ca